UNIVERSITÀ
DI PAVIA

Dipartimento di Biologia e Biotecnologie
"Lazzaro Spallanzani"

Laurea Magistralis in Molecular Biology and Genetics

Targetable pathways to modulate early fibrosis after ischemia in cardiac PDGFRα^{+} cells

Supervisor:
Professor. Maria Paola Santini

Experimental thesis by
Yasamin Nasiriyan

Academic Year 2025/2026

Abstract (English)

Cardiac fibrosis is a central pathological feature of cardiovascular diseases, contributing to impaired cardiac function and progression to heart failure. Platelet-derived growth factor receptor alpha (PDGFRα) cells play a critical role in fibrotic remodeling. Depending on the type and length of an injury, stromal cells expressing PDGFRα may induce different outcomes, regeneration and repair, and these outcomes likely relate to tissue restricted lineage commitment, and persistence of pathological cells in the tissue. However, the functional contribution of PDGFRα$^+$ cells to the balance between fibrosis and tissue repair remains not fully understood.

To study this, we employed an inducible PDGFRα$^+$ cell ablation model using PDGFRα–MerCreMer mice crossed with diphtheria toxin A (DTA) reporter mice. Myocardial ischemia reperfusion (I/R) injury was induced to replicate a clinical-like cardiac damage, followed by tamoxifen-mediated ablation of PDGFRα$^+$ cells. Cardiac function was assessed by echocardiography, while histological and immunofluorescence analyses were used to evaluate fibrosis, cardiomyocyte morphology, and vascular density.

PDGFRα$^+$ cell ablation resulted in a significant reduction in fibrotic remodeling, indicating a key role for these cells in extracellular matrix deposition. However, ablation was also associated with reduced angiogenesis and alterations in cardiomyocyte structure, suggesting impaired reparative processes. Spatial transcriptomic analyses of lineage traced PDGFRα$^+$ cells showed modulation of the membrane trafficking module regulated by clathrin-endosome formation as a possible molecular hub leading from reparative to fibrotic activation. *In vitro*, inhibition of this pathway decreased the expression of pathological profibrotic genes, while maintaining beneficial differentiation of PDGFRα$^+$ cells into contractile supporting cells, suggesting a membrane specific uncoupling between fibrosis and wound contraction properties of these cells.

Overall, these findings highlight the dual role of PDGFRα$^+$ cells in the injured heart, contributing both to pathological fibrosis and to tissue repair mechanisms. Targeting PDGFRα signaling may therefore represent a promising but complex therapeutic strategy, requiring precise signaling

modulation and timing treatment to balance fibrosis reduction with preservation of cardiac adaptive repair.

UNIVERSITÀ
DI PAVIA

Dipartimento di Biologia e Biotecnologie
"Lazzaro Spallanzani"

Laurea Magistralis in Molecular Biology and Genetics

Identificazione di vie molecolari bersagliabili per modulare la fibrosi precoce post-ischemica nelle cellule cardiache PDGFRα^{+}

Relatore:
Professor. Maria Paola Santini

Tesi di:
Yasamin Nasiriyan

Anno accademico 2025

Abstract (Italian)

La fibrosi cardiaca rappresenta una caratteristica patologica centrale delle malattie cardiovascolari, contribuendo alla compromissione della funzione cardiaca e alla progressione verso lo scompenso cardiaco. Le cellule che esprimono il recettore alfa del fattore di crescita derivato dalle piastrine (PDGFRα^{+}) svolgono un ruolo critico nel rimodellamento fibrotico. A seconda del tipo e della durata della lesione, le cellule stromali PDGFRα^{+} possono indurre esiti differenti, tra rigenerazione e riparazione; tali esiti sono probabilmente legati alla modulazione del lignaggio tessuto-specifico e alla persistenza di cellule patologiche nel tessuto.
Tuttavia, il contributo funzionale delle cellule PDGFRα^{+} nell'equilibrio tra fibrosi e riparazione tissutale non è ancora del tutto compreso.

Per studiare questo fenomeno, abbiamo impiegato un modello inducibile di ablazione cellulare PDGFRα^{+} utilizzando topi PDGFRα–MerCreMer incrociati con topi reporter per la tossina difterica A (DTA). Il danno da ischemia-riperfusione miocardica (I/R) è stato indotto per replicare un danno cardiaco di rilevanza clinica, seguito dall'ablazione delle cellule PDGFRα^{+} mediata dal tamoxifene. La funzione cardiaca è stata valutata tramite ecocardiografia, mentre analisi istologiche e di immunofluorescenza sono state utilizzate per valutare la fibrosi, la morfologia dei cardiomiociti e la densità vascolare.
L'ablazione delle cellule PDGFRα^{+} ha determinato una significativa riduzione del rimodellamento fibrotico, indicando un ruolo chiave di queste cellule nel deposito della matrice extracellulare. Tuttavia, l'ablazione è stata associata anche a una ridotta angiogenesi e ad alterazioni nella struttura dei cardiomiociti, suggerendo una compromissione dei processi riparativi.

Analisi di trascrittomica spaziale su cellule PDGFRα^{+} (sottoposte a *lineage tracing*) hanno mostrato che la modulazione del modulo del traffico di membrana, regolato dalla formazione dell'endosoma-clatrina, agisce come un possibile snodo molecolare nel passaggio dall'attivazione riparativa a quella fibrotica.
In vitro, l'inibizione di questa via ha diminuito l'espressione di geni profibrotici, mantenendo al contempo il differenziamento delle cellule PDGFRα^{+} in cellule di supporto contrattile; ciò

suggerisce un disaccoppiamento specifico, a livello di membrana, tra le proprietà di patologiche fibrosi e quelle benefiche di contrazione della ferita proprie di queste cellule.

Nel complesso, questi risultati evidenziano il duplice ruolo delle cellule PDGFRα^{+} nel cuore danneggiato, contribuendo sia alla fibrosi patologica che ai meccanismi di riparazione tissutale necessary per mantenere l'integrita' del tessuto. Mirare alla segnalazione di PDGFRα potrebbe quindi rappresentare una strategia terapeutica promettente ma complessa, che richiede una precisa modulazione del segnale e una tempistica del trattamento accurata per bilanciare la riduzione della fibrosi con la preservazione della riparazione adattativa cardiaca.

ABSTRACT (ENGLISH) **2**

ABSTRACT (ITALIAN) **5**

1.1 THE MAMMALIAN HEART 10

1.2 CARDIOVASCULAR DISEASE 13

1.2.1 CORONARY HEART DISEASE 13

1.3 FIBROSIS IN CARDIOVASCULAR SYSTEMS 15

1.3.1 Mechanism of fibrotic response *17*

1.3.2 Molecular markers of fibrotic and myofibroblast activation *19*

1.3.3 Balance between fibrosis and revascularization *20*

1.4 PDGFRA SIGNALING IN THE CARDIOVASCULAR SYSTEM 21

1.4.1 The dichotomous role of PDGFRα *24*

1.5 THE SIGNIFICANCE OF ANIMAL MODELS IN CARDIOVASCULAR DISEASE RESEARCH 25

1.6 CRE/LOXP SYSTEM AND ABLATION 25

1.6.1 MerCreMer system *27*

1.7 ASSESSMENT OF CARDIAC FUNCTION BY ULTRASOUND IN ANIMAL MODELS 28

CHAPTER 2 - AIM OF THE WORK **30**

CHAPTER 3 - MATERIAL AND METHODS **31**

3.1 MOUSE STRAINS AND BREEDING 31

3.2 ISCHEMIA–REPERFUSION (I/R) SURGERY 32

3.3 TAMOXIFEN-INDUCED CELL ABLATION 32

3.4 ECHOCARDIOGRAPHIC ASSESSMENT 34

3.5 Tissue Collection and Processing 35

3.6 Picrosirius Red Staining and Fibrosis Quantification 36

3.7 Immunofluorescence staining 38

3.8 Confocal microscopy 40

3.8 Flow Cytometry 40

3.9 Porcine Tissue Collection 41

3.10 Porcine Cardiac Cell Culture 42

3.11 TGFB and Chlorpromazine Treatment 43

3.12 RNA Isolation, cDNA analysis and RT-qPCR 44

CHAPTER 4 - RESULTS **51**

4.1 Experimental design and timeline for inducible cell ablation following ischemia–reperfusion injury 51

4.2 Validation of PDGFRA$^+$ cell ablation following tamoxifen administration 52

4.3 Inducible cell ablation exacerbates systolic dysfunction following ischemia–reperfusion injury 54

4.4 Inducible cell ablation reduces fibrotic remodeling after I/R 55

4.5 Effects of inducible cell ablation on cardiomyocyte morphology and vascular density under physiological and pathological conditions 57

4.6 Chlorpromazine modulates TGFB-induced profibrotic gene expression in porcine PDGFRα + cells 59

4.7 Chlorpromazine attenuates TGFB-induced profibrotic gene expression in porcine cardiac tissue 61

CHAPTER 5 - DISCUSSION **63**

5.1 PDGFRA+ CELLS CONTRIBUTE TO CARDIAC HOMEOSTASIS UNDER BASAL CONDITIONS . 63

5.2 ABLATION OF PDGFRA+ CELLS REDUCE FIBROSIS BUT IMPAIRS CARDIAC REPAIR AFTER I/R 64

5.3 PDGFRA+ CELLS AS REGULATORS OF THE BALANCE BETWEEN FIBROSIS AND REVASCULARIZATION 64

5.4 CLATHRIN-DEPENDENT TRAFFICKING AS A REGULATOR OF FIBROTIC SIGNALING 65

5.5 SPATIAL COMPARTMENTALIZATION OF TGFB SIGNALING 65

5.6 FUNCTIONAL IMPLICATIONS OF SELECTIVE SERPINE1 REGULATION 66

5.7 LIMITATIONS OF THE STUDY 66

CONCLUSION 67

REFERENCES..... 68

ACKNOWLEDGEMENTS 73

Chapter 1 - Introduction

1.1 The mammalian heart

Across mammalian species, the heart remains mostly conserved in both structure and function. This evolutionary stability reflects strong optimization in fluid mechanics, in the organization of the circulatory system and preservation of the mechano-transduction forces (1). The mammalian heart consists of four chambers, two atria and two ventricles which are organized into right and left pumps (Figure 1). The heart circulates blood to support both oxygen delivery to tissues and removal of waste. This double circulation consists of pulmonary and systemic circulation (1). The right atrium receives deoxygenated blood, then passes it to the right ventricle by tricuspid valve, which pumped it to the lungs by pulmonary artery for oxygenation (2), which is called pulmonary circulation. The oxygenated blood returns to the left atrium and passes through the mitral valve into the left ventricle, which ejects it into the whole body through the major artery, the Aorta, supplying oxygen and nutrient all organs via systemic circulation.

Cardiac function is governed by the cardiac cycle, which consists of alternating phases of contraction (systole) and relaxation (diastole) (Figure 1.1). The heart acts as a muscular pump that generates the force required to circulate blood throughout the body. Its mechanical activity alternates between contraction and relaxation phases. During systole, cardiac muscle contraction increases intramyocardial pressure, while during diastole relaxation reduces this pressure and allows coronary blood flow to occur more effectively (3) . These processes are tightly regulated by intrinsic cardiac mechanisms as well as neural and hormonal inputs, enabling the heart to adapt rapidly to changing physiological and pathological demands (4).

Unidirectional blood flow through the heart is maintained by four principal valves: the atrioventricular valves (mitral and tricuspid) and the semilunar valves (aortic and pulmonary). Proper valve function is essential to prevent blood regurgitation and to preserve cardiac efficiency (5).

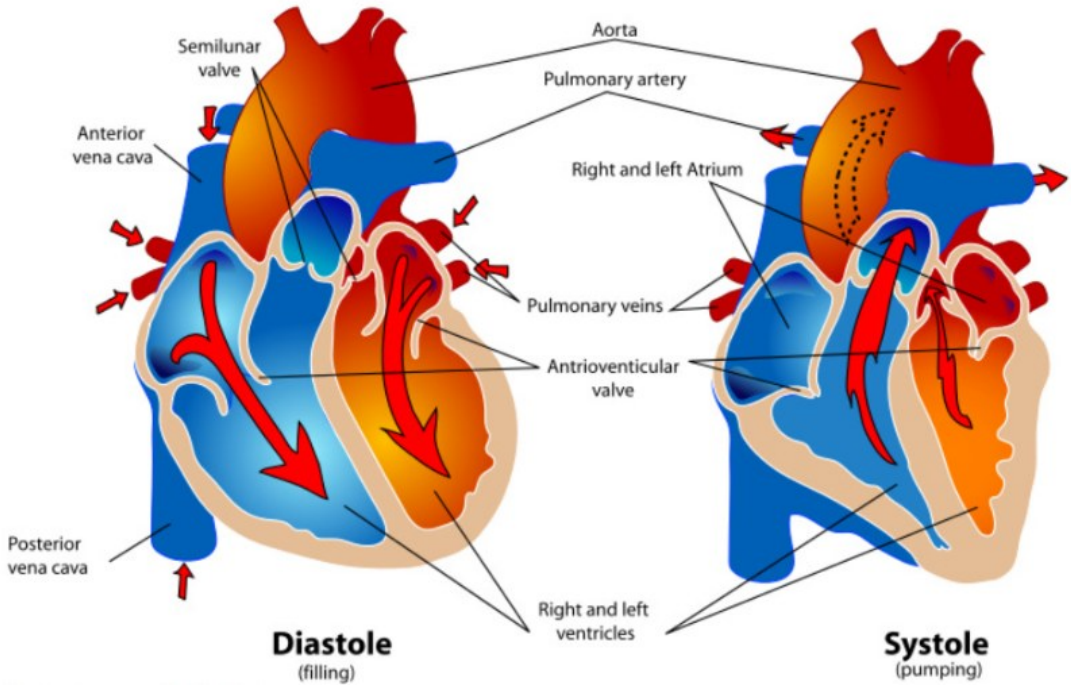

Figure 1.1. This diagram illustrates the different anatomical parts of the heart and the filling and pumping cycles in a healthy heart. The image is from Mariana Ruiz, and it is part of the Common Creatives repository of Wikimedia

The left ventricle is thicker than the right ventricle due to the mechanical forces required to drive blood to the whole body (6).

Beyond its anatomical organization, the mammalian heart is a complex multicellular organ composed of several specialized cell types (7) (Figure 1.2), including cardiomyocytes which are the dominant contractile cells responsible for force generation and rhythmic contraction (8), endothelial cells which line the internal part of the entire vasculature and of the endocardial surface, where they regulate nutrient and oxygen exchange, maintain vascular integrity, and participate in paracrine signaling (7), and cardiac fibroblasts, located within the myocardial interstitium, which play a central role in producing and remodeling the extracellular matrix, thereby contributing to both structural support and pathological remodeling (9) (Figure 1.2). Other groups of cells include mural cells, consisting of pericyte and vascular smooth muscles cells, which

contribute to protection and contractility of the medium and big size arteries (10), the immune cells, the epicardial fat cells, and neurons (7).

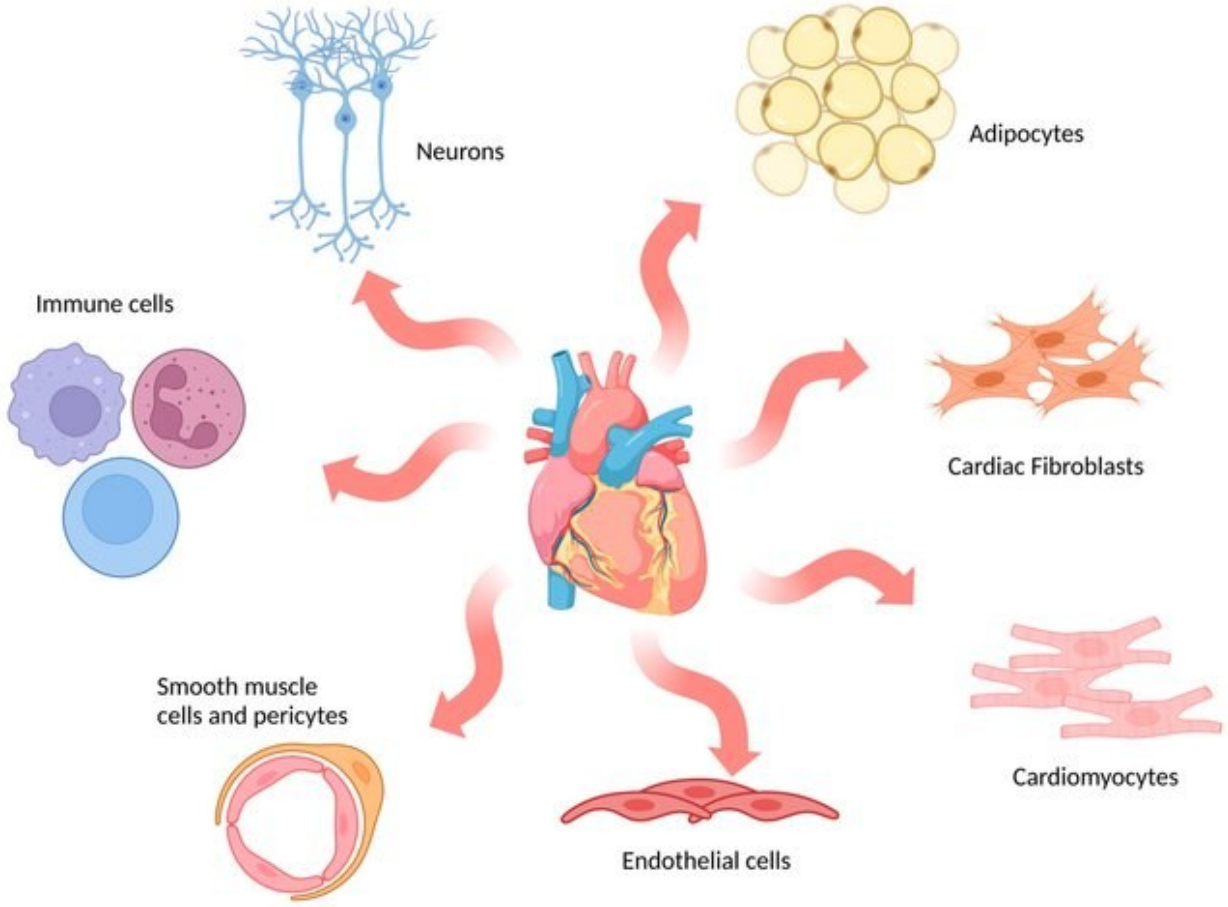

Figure 1.2. Schematic representation of main cell types in human heart. . This image is from Baena-Montes J and co-workers (11). This article is an open access article distributed under the terms and conditions of the Creative Commons Attribution (CC BY) license.

Disruption of the coordinated structural, cellular, and functional organization of the heart underlies many forms of cardiovascular disease, including heart failure and pathological remodeling (12).

1.2 Cardiovascular disease

Cardiovascular diseases (CVDs) comprise several disorders of the heart muscle and blood vessels, including conditions that impair myocardial perfusion, vascular integrity, and cardiac function. stroke and coronary heart disease are the two main contributors of morbidity and mortality in cardiovascular disease.(13). CVDs remain the leading cause of death worldwide, the world health organization (WHO) reported that in 2021, approximately 20.5 million people die from CVDs, accounting for nearly one-third of all global mortality. About 80% of deaths happen in low-income and middle-income countries (14).

Beyond mortality, CVD remains a major global challenge, it is a burden on the health system as it contributes to healthcare costs, long disability, and loss of productivity. The etiology of cardiovascular disease is strongly influenced by modifiable risk factors, including smoking, excessive alcohol consumption, physical inactivity, hypertension, diabetes mellitus, obesity, and dyslipidemia(15).

Cardiovascular diseases are grouped into major types including coronary artery disease, cerebrovascular disease, peripheral artery diseases, and aortic atherosclerosis (16). Among these, coronary artery disease is the most prevalent and clinically significant form.

1.2.1 Coronary heart disease

Coronary artery disease (CAD) remains a leading cause of morbidity and mortality worldwide (17). It is a condition characterized by narrowing or blockage of coronary arteries, which supply myocardium with oxygen-rich blood. The most common underlying pathological process in CAD is atherosclerosis, a chronic inflammatory condition marked by lipid accumulation, plaque formation, and progressive arterial wall remodeling, ultimately leading to luminal narrowing and impaired coronary blood flow (18).

Clinically, coronary artery disease ranges from stable angina to acute coronary syndromes and eventually leads to arrhythmias, myocardial infarction, and heart failure. Repeating injury and chronic ischemia leads to fibrosis, ventricular remodeling, and heart failure (19).

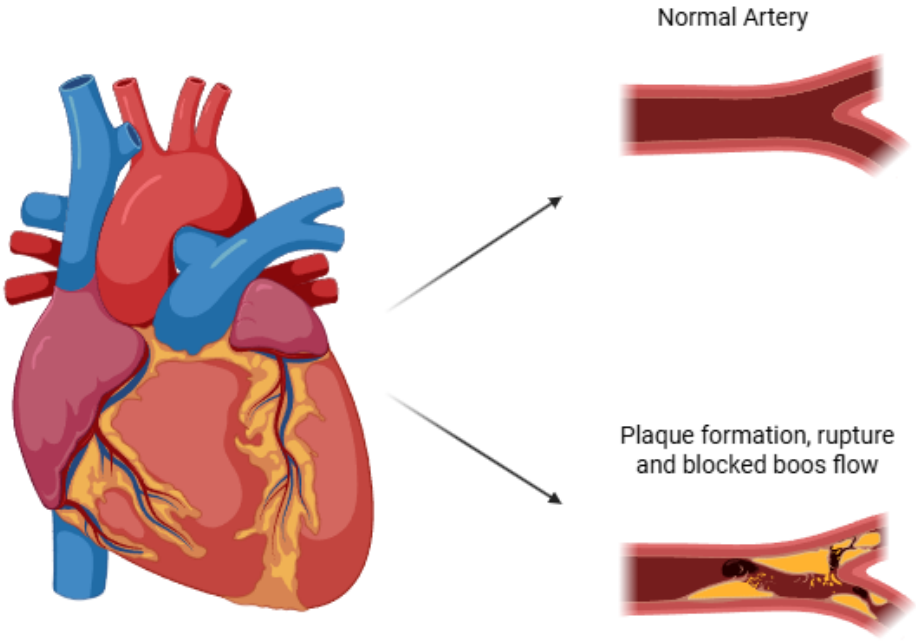

Figure 1.3. Schematic representation of differences between a healthy artery and a artery with CAD. This picture is made by Biorender and can be used for academic illustrations.

Diagnosis of coronary artery disease relies on a combination of clinical assessment and imaging modalities, including electrocardiography, echocardiography, stress testing, coronary angiography, computed tomography (CT), and magnetic resonance imaging (MRI), which together allow evaluation of myocardial perfusion, cardiac structure, and functional impairment (20).

1.3 Fibrosis in cardiovascular systems

Cardiac fibrosis is a pathological condition characterized by accumulation of extracellular matrix proteins (ECM) within myocardium. Cardiac fibroblasts play a central role in both physiological tissue repair and pathological remodeling by releasing several ECM components, including collagens, fibronectin, and proteoglycans. Different types of cardiac injury can lead to cardiac fibrosis including ischemia, pressure overload, inflammation, and aging. Progressive fibrosis contributes to increased ventricular stiffness, impaired contractility, electrical conduction abnormalities, and ultimately the development of heart failure.

Cardiac fibrosis is associated with both systolic and diastolic dysfunction. Because the adult mammalian heart has minimal regenerative capacity, extensive cardiomyocyte death after myocardial infarction triggers reparative fibrosis, formation of a scar rich in collagen that preserves ventricular structural integrity and prevents wall rupture and bleeding. However, while reparative fibrosis is initially protective, excessive or persistent fibrosis can compromise cardiac function (21).

In contrast to post-infarction scarring, chronic pathological stresses such as pressure overload, volume overload, metabolic disease, or aging induce interstitial and perivascular fibrosis even without myocardial infarction, these forms of fibrosis are characterized by diffuse collagen deposition throughout the myocardial interstitium and around the coronary vasculature, leading to progressive myocardial stiffening and impaired relaxation.

Myofibroblasts are the principal effector cells responsible for pathological ECM accumulation during cardiac fibrosis. The key effector cells in fibrosis are activated myofibroblasts, which arise from resident interstitial fibroblast populations. Other cardiac cell types supporting fibrotic response by releasing inflammatory mediators, proteases, and matricellular proteins, or by directly influencing fibroblast behavior include cardiomyocytes, endothelial cells, pericytes, macrophages, lymphocytes, and mast cells (22).

In addition to mechanical and ischemic stressors, toxic agents such as alcohol or anthracyclines and metabolic disorders including diabetes and obesity have been shown to promote ongoing fibrotic remodeling of the myocardium across human and animal studies (23).

Cardiac fibrosis can be classified into distinct subtypes based on its anatomical distribution (Figure 1.4). Replacement fibrosis is a result of myocardial infarction when a large amount of cardiomyocyte loss leads to replacement fibrosis (Figure 1.4A). Interstitial fibrosis is a deposition of collagen in interstitial space (Figure 1.4B). Perivascular fibrosis is defined by expansion of the adventitial extracellular matrix surrounding the coronary vasculature (Figure 1.4C). Studies in human cardiac fibrosis, including chronic transplant rejection, demonstrate that the majority of collagen-producing cells originate from resident cardiac cell populations rather than circulating progenitors (Figure 1.4D) (23).

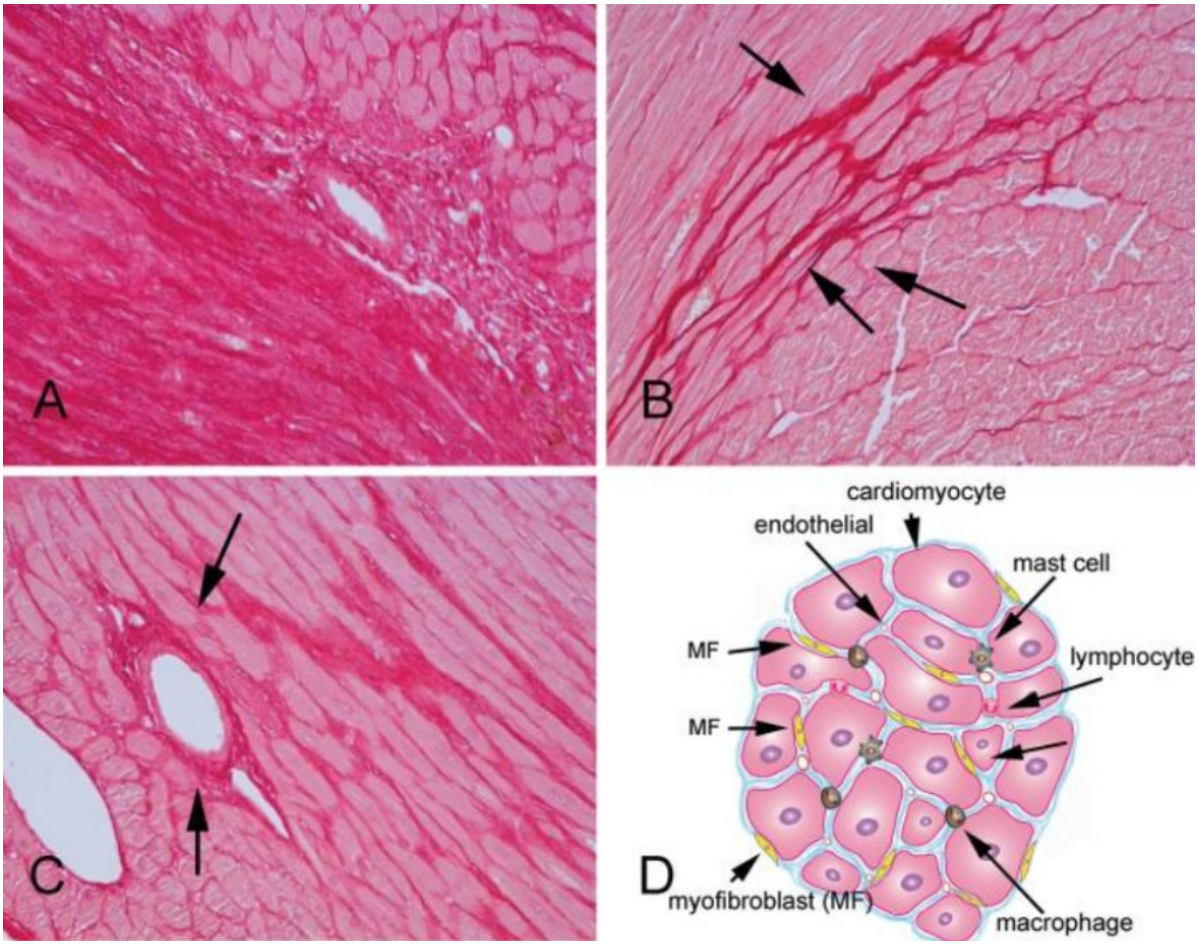

Figure 1.4. Distinct forms of cardiac fibrosis: (A) replacement fibrosis, (B) interstitial fibrosis, (C) perivascular fibrosis, and (D) myofibroblasts as the primary effector cells driving fibrotic

remodeling. This is an image from the pathogenesis of cardiac fibrosis; this article is licensed under a Creative Commons Attribution 4.0 International License (23) (24).

Fibrosis is driven by different pro-fibrotic signals that activate fibroblasts and promote extracellular matrix deposition. TGF-β/Smad2/3 is the central pathway. Additional pathways, including PDGF-PDGFRα signaling, angiotensin II, IL-11, Wnt/β-catenin, Notch, and YAP/TAZ-mediated mechano-transduction, contribute to fibroblast proliferation, migration, and matrix production. Together, these pathways coordinate the persistent and maladaptive ECM accumulation that characterizes pathological cardiac fibrosis (21).

1.3.1 Mechanism of fibrotic response

There are several mechanisms inducing fibrosis, which include endothelial to mesenchymal transition (EndMT) and TGFβ signaling pathways.

Endothelial to mesenchymal transition (EndMT)

Endothelial-to-mesenchymal transition (EndMT) is a process in which endothelial cells progressively lose their endothelial characteristics such as cell junctions and polarity and acquire a mesenchymal-like phenotype, such as that of myofibroblasts or smooth muscle cells. While EndMT is essential during embryonic development, evidence suggests that it also contributes to adult cardiovascular pathologies, including atherosclerosis, pulmonary hypertension, valvular heart disease, and fibroelastosis. Because of its role in generating fibrogenic cells, modulating EndMT represents a promising therapeutic strategy for cardiovascular disease (25).

TGFβ signaling pathway

Transforming growth factor-β (TGF-β) signaling is a central driver of fibrotic remodeling in the cardiovascular system. Following cardiac injury, TGF-β is rapidly activated and orchestrates fibroblast activation, myofibroblast differentiation, and extracellular matrix (ECM) deposition. While transient TGF-β activation is essential for wound healing and tissue repair, sustained or excessive signaling promotes pathological fibrosis, leading to myocardial stiffening and progressive cardiac dysfunction (26).

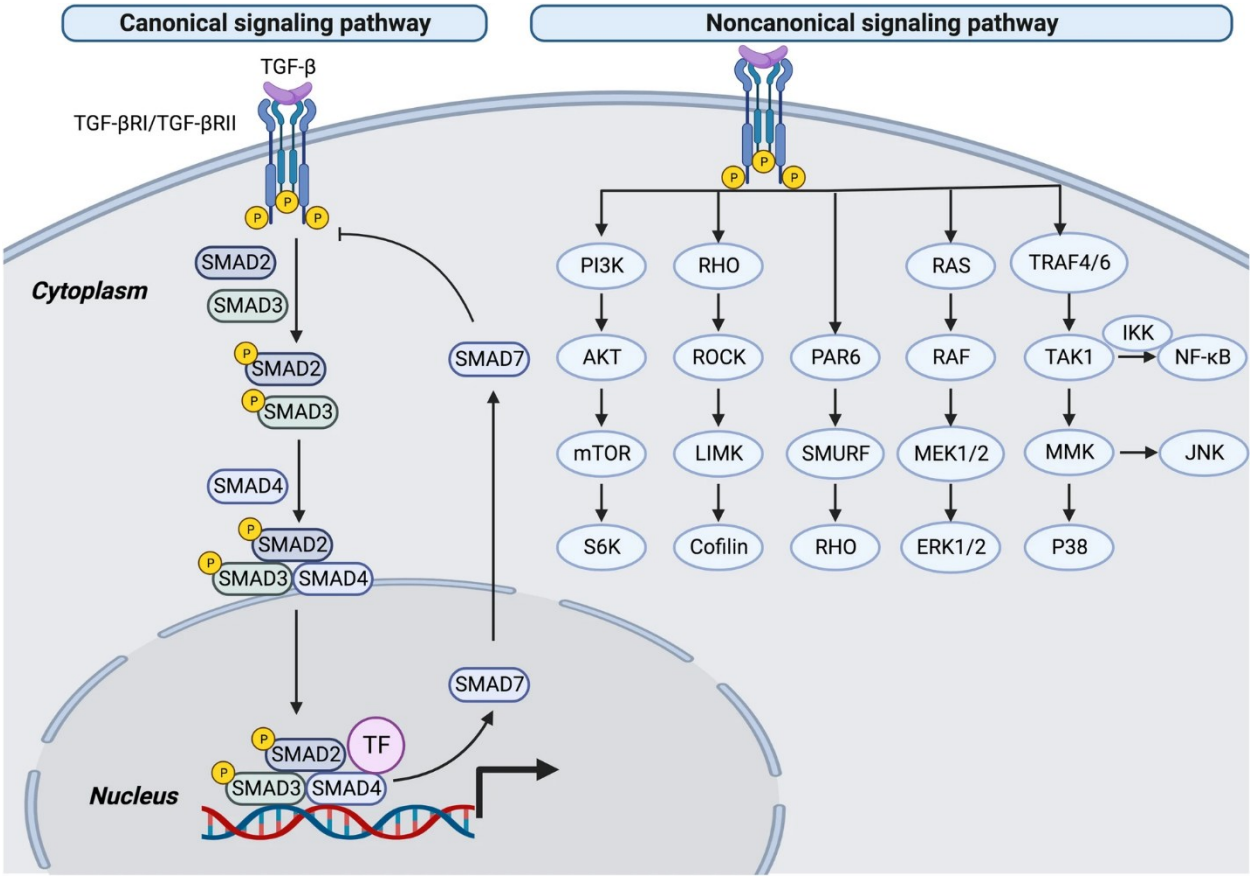

Figure 1.5. Canonical and non-canonical TGF-β signaling pathway. Picture is from Wikimedia common website, and it is licensed under a Creative Commons Attribution.

The canonical TGF-β signaling pathway is mediated through Smad proteins. Upon ligand binding, TGF-β receptor II phosphorylates and activates TGF-β receptor I, leading to phosphorylation of Smad2 and Smad3. These activated Smads form a complex with Smad4 and translocate into the nucleus, where they regulate the transcription of profibrotic genes, including collagens, fibronectin, connective tissue growth factor (CTGF), and α-smooth muscle actin. Through this mechanism, TGF-β directly promotes fibroblast-to-myofibroblast differentiation and extracellular matrix accumulation (27).

In addition to the canonical Smad-dependent pathway, TGF-β activates several non-canonical signaling cascades, including MAPK, PI3K/AKT, and RhoA/ROCK pathways. These non-canonical pathways modulate cytoskeletal dynamics, cell migration, survival, and mechanosensitive responses, thereby reinforcing fibroblast activation and fibrotic remodeling. Crosstalk between canonical and non-canonical signaling allows TGF-β to integrate mechanical, inflammatory, and metabolic cues during cardiac injury (28).

TGF-β signaling is a key determinant of myofibroblast persistence within the injured myocardium. By promoting resistance to apoptosis and sustaining ECM production, TGF-β contributes to the stabilization of the fibrotic scar. However, prolonged myofibroblast activation prevents proper resolution of the repair process and leads to maladaptive interstitial and perivascular fibrosis. Consequently, dysregulated TGF-β signaling is a major contributor to the transition from adaptive wound healing to chronic heart failure (29).

1.3.2 Molecular markers of fibrotic and myofibroblast activation

During cardiac injury, fibroblast activation and myofibroblast differentiation are accompanied by changes in the expression of several fibrosis-associated genes. These molecular markers are commonly used to evaluate the activation state of stromal cells and the progression from reparative remodeling toward pathological fibrosis.

SERPINE1 (plasminogen activator inhibitor-1, PAI-1) is a well-established downstream target of TGFβ signaling and an important regulator of extracellular matrix turnover. Increased SERPINE1

expression promotes matrix accumulation and is associated with the development of fibrotic diseases (30).

COL1A1 encodes the α1 chain of type I collagen, one of the principal extracellular matrix proteins deposited during cardiac fibrosis (31). ACTA2 is a marker of myofibroblast differentiation, which encodes α-SMA. Myofibroblast differentiation is characterized by de novo expression of α-smooth muscle actin (α-SMA), which is incorporated into stress fibers and contributes to cellular contractility during tissue repair and fibrosis (32). CNN1 encodes calponin-1, an actin-binding cytoskeletal protein involved in the regulation of smooth muscle contractility. Because its expression increases during smooth muscle differentiation, CNN1 is commonly used as a marker of contractile cell maturation and differentiation (33).

Together, these genes provide complementary information about the fibrotic response: SERPINE1 and COL1A1 mainly reflect extracellular matrix remodeling and deposition, whereas ACTA2 and CNN1 indicate the development of a contractile myofibroblast-like phenotype. Therefore, their analysis by RT-qPCR allows the evaluation of how TGFβ and clathrin-mediated trafficking influence distinct aspects of PDGFRα^{+} cell activation.

1.3.3 Balance between fibrosis and revascularization

Revascularization is the restoration of blood flow to ischemic myocardium through the formation of new vessels and remodeling of existing vascular networks. This is an important process for maintaining oxygen and nutrient delivery to cardiomyocytes and for tissue support after myocardial infarction or ischemia reperfusion injury. Revascularization occurs through coordinated mechanisms, including angiogenesis, arteriogenesis, and vasculogenesis, which together contribute to vascular repair and adaptation in the injured heart (34).

Following myocardial infarction, the heart needs to gain a balance between fibrosis, which stabilizes damaged tissue and revascularization, which restores oxygen supply to the surviving myocardium. Although fibrosis provides support after loss of cardiomyocyte and prevents ventricular rupture, excessive and persistent ECM creates poorly perfused

environments that impair cardiac function (21). Angiogenic responses after myocardial infarction may occur as a delayed process, and VEGF expression is induced under hypoxic/ischemic conditions. (35), Therefore, coordinated regulation of fibrotic repair and vascular regeneration is critical for optimal cardiac healing and functional recovery.

1.4 PDGFRα signaling in the cardiovascular system

Platelet derived growth factor receptor (PDGFR) family are members of receptor tyrosine kinase super family and play an essential role in cell proliferation, migration, survival, and differentiation. The PDGFR family consists of two isoforms, PDGFRα and PDGFRβ; they form homodimers or heterodimers upon binding to ligands. They have 5 different ligands including PDGF AA, PDGF BB, PDGF AB, PDGF CC, and PDGF DD, each exhibiting distinct receptor-binding specificities and biological effects (figure 1.6) (36).

PDGFRα consists of an extracellular ligand-binding domain, a single transmembrane domain, and an intracellular tyrosine kinase domain (Figure 1.6). When it binds its ligand, it goes through dimerization leading to autophosphorylation of specific tyrosine residue within the intracellular domain. It activates multiple downstream pathways including PI3K/AKT pathway, which promotes cell survival; the MAPK/ERK pathway, which drives proliferation; the PLCγ pathway, which regulates intracellular calcium signaling and cell migration; and the JAK/STAT pathway, which modulates differentiation, inflammation, and gene transcription (37) (38).

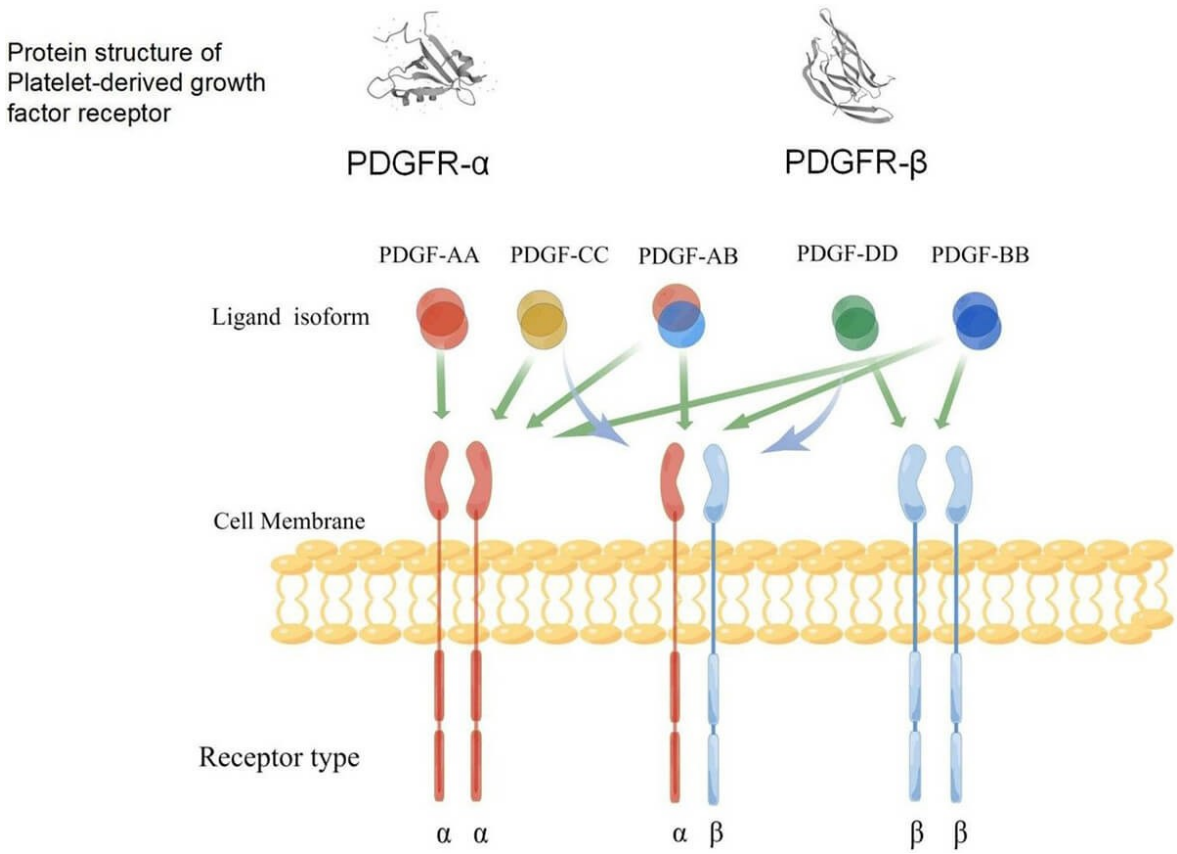

Figure 1.6. Schematic diagram of PDGF ligands binding to the two isoforms of PDGF receptors, α and β (39). This is an open-access article distributed under the terms of the Creative Commons Attribution License (CC BY).

PDGFRα is broadly expressed in mesenchymal cell populations during development, with particularly strong expression in subsets of mesenchymal progenitors in tissues such as the lung, skin, intestine, and neural crest-derived structures. PDGF-A/PDGFRα signaling plays important roles in epithelial–mesenchymal interactions, promoting the proliferation, migration, and spreading of PDGFRα-positive mesenchymal cells during organogenesis and morphogenesis. These processes contribute to the development of multiple organs, including the lung, intestine, skin, gonads, kidney, palate, teeth, and cardiac outflow tract. (40). PDGFRα marks cardiac mesenchymal progenitor populations with fibroblast and smooth muscle lineage potential. In the developing and adult heart, PDGFRα^{+} cells are found in epicardial-derived and interstitial compartments, where they may contribute to cardiac fibroblast populations involved in tissue

repair. Experimental evidence also suggests that PDGFRα signaling participates in cardiac fibroblast activation and collagen deposition, implicating this pathway in fibrotic remodeling after myocardial injury. (41).

PDGF/PDGFR signaling is strongly implicated in mesenchymal-cell responses involved in tissue repair, vascular remodeling, cancer-associated stromal activation, and fibrotic disease. In fibroblasts, PDGF acts as a potent mitogenic and chemotactic signal, promoting migration toward sites of injury and supporting proliferative expansion during wound healing. PDGF signaling also contributes to extracellular matrix remodeling by regulating fibroblast activation and collagen production. In the heart, experimental evidence indicates that PDGFRα signaling participates in post-infarction fibrotic remodeling, since PDGFRα blockade reduces collagen deposition in the infarcted myocardium. However, when PDGF/PDGFR signaling becomes persistent or dysregulated, it can drive excessive connective tissue production, scarring, and fibrosis; accordingly, constitutive activation of PDGFRα has been shown to disrupt connective tissue development and promote systemic fibrosis. (42).

Therapeutic targeting of PDGFRα has emerged as a promising strategy across oncology, fibrotic disorders, and regenerative cardiovascular medicine. Because PDGFRα is a receptor tyrosine kinase, several clinically approved tyrosine kinase inhibitors (TKIs), like imatinib, can block PDGFRα signaling. Experimental studies demonstrate that reducing PDGFRα signaling can reduce fibroblast proliferation, limit myofibroblast differentiation, and decrease maladaptive collagen deposition. These findings highlight PDGFRα as a potential therapeutic target to decrease cardiac fibrosis (21) (36).

Although PDGFRα signaling is in part implicated in pathological responses, making it a major contributor to maladaptive cardiac fibrosis. several studies reveal that PDGFRα marks key mesenchymal and epicardium-derived progenitor cells that participate in cardiac development, vascular support, and potential regenerative processes. This duality of action poses PDGFRα signaling as both a therapeutic target for anti-fibrotic intervention and a lever for regenerative strategies in the injured heart.

1.4.1 The dichotomous role of PDGFRα

In our laboratory, we observed that PDGFRα signaling plays a dual and context-dependent role in the adult skeletal muscle and in human arteries (43, 44), contributing to both tissue repair and pathological remodeling. In the heart, several manuscripts showed that PDGFRα identifies a population of resident mesenchymal cells that includes progenitor-like cells with the capacity to support cardiac repair through paracrine signaling, vascular stabilization following myocardial injury, collagen re-organization and increased myocardial contractility (44) (45) (46) (47) (48). In parallel, it has been shown that distinct PDGF ligands and receptors can exert protective effects when appropriately regulated. Indeed, endothelial cell–derived PDGF-BB promotes cardiomyocyte survival after myocardial infarction by activating PDGFR-β–dependent PI3K/Akt signaling, thereby reducing apoptosis and preserving systolic function. Importantly, when PDGF-BB delivery was spatially and temporally controlled, cardiac function improved without inducing fibroblast proliferation, fibrosis, excessive angiogenesis, or inflammation (49). Noseda and coworkers observed that injection of fluorescently labelled PDGFRa cardiac cells induced tissue revascularization after myocardial infarction induction(50). Taken together, these findings support the dual nature of PDGF signaling. Although the detailed mechanisms at cellular and molecular level is unknown, different hypotheses started to refer to extension and chronicity of the injury, and tissue-specific lineage determination as possible causes of this duality of function.

Our studies clearly indicate that at early phases after damage, activation of PDGFRα^{+} cells contribute to wound healing and preservation of tissue integrity. However, when PDGFRα signaling is sustained or dysregulated, it promotes fibroblast proliferation, differentiation into myofibroblasts, and excessive extracellular matrix deposition. This persistent activation leads to maladaptive fibrotic remodeling, increased progression toward tissue functional failure. Thus, PDGFRα functions as a critical regulator at the interface between reparative responses and pathological fibrosis (43) (44).

1.5 The significance of animal models in cardiovascular disease research

Animal models are great tools in cardiovascular disease research because they enable the investigation of complex cardiac pathophysiology mechanisms in a whole-organism context that cannot be fully replicated in vitro. Cardiovascular diseases involve tightly interconnected processes, such as hemodynamic stress, neurohumoral regulation, inflammation, fibrosis, and vascular remodeling that require an intact circulatory and immune system for accurate study. Animal models allow researchers to examine how these mechanisms interact over time, from disease initiation to progression and eventual heart failure (51).

1.6 Cre/loxP system and ablation

Because of their easy laboratory maintenance, short reproductive time length, and availability of tools for their genome manipulation, mice represent an advantageous *in vivo* system to study human disease mechanisms. Genetically modified mouse models are available in different repository distributors worldwide, allowing them to study timely and spatially regulated genes of interest. Among them the Cre/loxP system represents one of the most powerful genetic tools for manipulating genes of interest with precise spatial and temporal control. Cre recombinase is a site-specific enzyme that recognizes a defined DNA sequence known as **loxP** and mediates recombination between two loxP sites, resulting in deletion, inversion, or rearrangement of the intervening DNA segment. A loxP site is 34 base pairs in length and consists of two 13 bp palindromic repeats flanking an 8 bp asymmetric core sequence.

The Cre/loxP system relies on two essential genetic components: a mouse line expressing Cre recombinase under the control of a specific promoter or enhancer, and a mouse line in which the gene of interest is flanked by loxP sites (floxed). Breeding these two strains generates conditional mutant mice in which gene recombination occurs selectively in specific cell types or at defined developmental stages. Thus, the specificity and timing of recombination are dictated by the regulatory elements driving Cre expression (52).

This conditional approach allows gene function to be manipulated in a tissue- or cell type-specific manner, while preserving normal gene activity in other tissues. By using Cre recombinase as a genetic inactivation switch, loxP-flanked genes can be selectively deleted in defined cell populations. This strategy is particularly useful when conventional global knockout approaches cause early developmental defects or lethality, preventing the analysis of gene function in adult tissues. (53).

At the molecular level, Cre/loxP recombination is a highly coordinated process (Figure 1.7). It begins when two Cre recombinase molecules recognize and bind to a loxP site. Once bound, two Cre/loxP complexes come together in an antiparallel orientation, forming a stable tetramer that brings the two loxP sites into close alignment. Cre then cuts one DNA strand from each loxP site, creating an intermediate in which the enzyme remains attached to the DNA through a temporary linkage. This is followed by a controlled strand exchange and ligation step that produces a four-way DNA structure known as a Holliday junction. A final isomerization step determines which Cre molecules perform the second round of strand cleavage, ultimately resolving the Holliday junction and completing the recombination event. Through this highly orchestrated mechanism, Cre mediates efficient and site-specific DNA recombination at loxP sites (54).

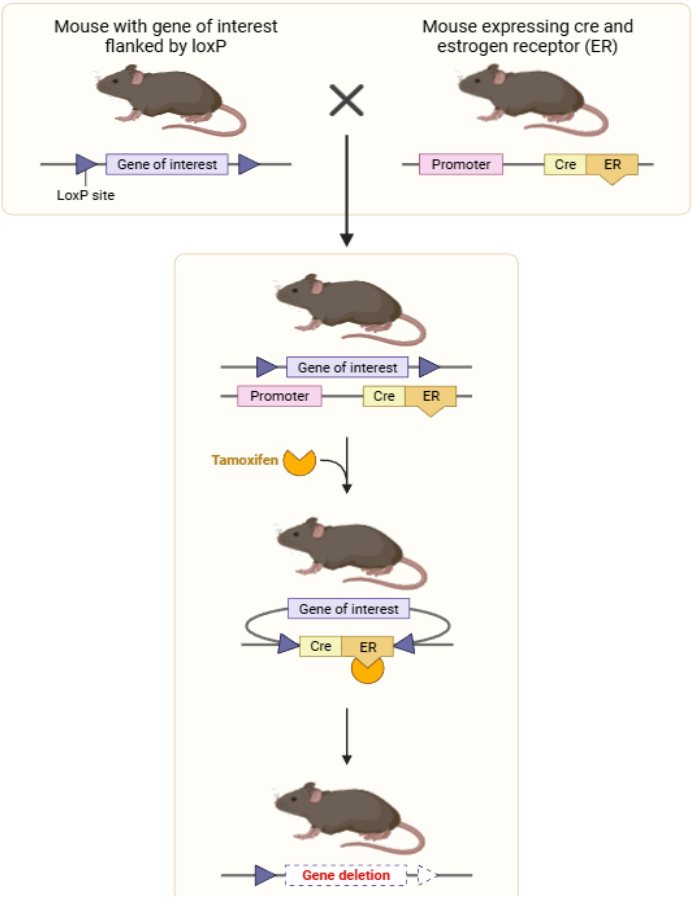

Figure 1.7. Schematic representation of the inducible Cre loxP system and its activation by tamoxifen. This figure is made by Biorender

1.6.1 MerCreMer system

The MerCreMer system is a tamoxifen-inducible Cre recombinase strategy in which Cre is fused to two mutated estrogen receptor ligand-binding domains (Mer), positioned at the N- and C-terminal domains of the enzyme. In the absence of tamoxifen, these modified estrogen receptor domains sequester the Cre recombinase in the cytoplasm, thereby preventing unintended genomic recombination. Upon administration of tamoxifen, the MerCreMer fusion protein undergoes conformational activation and translocate into the nucleus, where Cre mediates recombination at

loxP-flanked target sites, resulting in gene excision or activation depending on the genetic design of the allele (Figure 1.7).

Importantly, the estrogen receptor domains used in the MerCreMer construct are mutated to render the system insensitive to endogenous estrogens while remaining highly responsive to tamoxifen. This modification ensures tight temporal control of Cre activity. When driven by a cell- or tissue-specific promoter, the MerCreMer system enables selective, time-dependent inducible recombination, making it a powerful tool for studying gene function in the adult tissues (55).

1.7 Assessment of Cardiac Function by Ultrasound in Animal Models

Non-invasive assessment of cardiac structure and function is essential for studying cardiovascular disease progression and therapeutic interventions in experimental models. High-resolution ultrasound imaging, commonly referred to as echocardiography, is the most widely used technique for evaluating cardiac function in small and large animal models (Figure 1.8). Echocardiography enables real-time visualization of cardiac chambers, ventricular wall motion, and blood flow dynamics without the need for surgical intervention, allowing repeated measurements in the same animal over time (56).

In rodent models, high-frequency ultrasound systems provide sufficient spatial and temporal resolution to accurately assess left ventricular dimensions and systolic performance. Key functional parameters derived from echocardiography include left ventricular end-diastolic and end-systolic diameters, ejection fraction, fractional shortening, stroke volume, and cardiac output. These measurements are commonly used to quantify cardiac contractility and assess systolic and diastolic dysfunctions following myocardial infarction, pressure overload, or genetic manipulation. Doppler and tissue Doppler imaging further enable evaluation of diastolic function and hemodynamic changes by measuring ventricular filling patterns, myocardial relaxation, and blood flow velocities. In larger animal models, such as pigs, echocardiography closely parallels clinical cardiac imaging and allows comprehensive assessment of ventricular performance, valvular function, and remodeling. Because of its non-invasive nature, reproducibility, and

translational relevance, echocardiography represents a cornerstone technique for functional phenotyping in preclinical cardiovascular research (57).

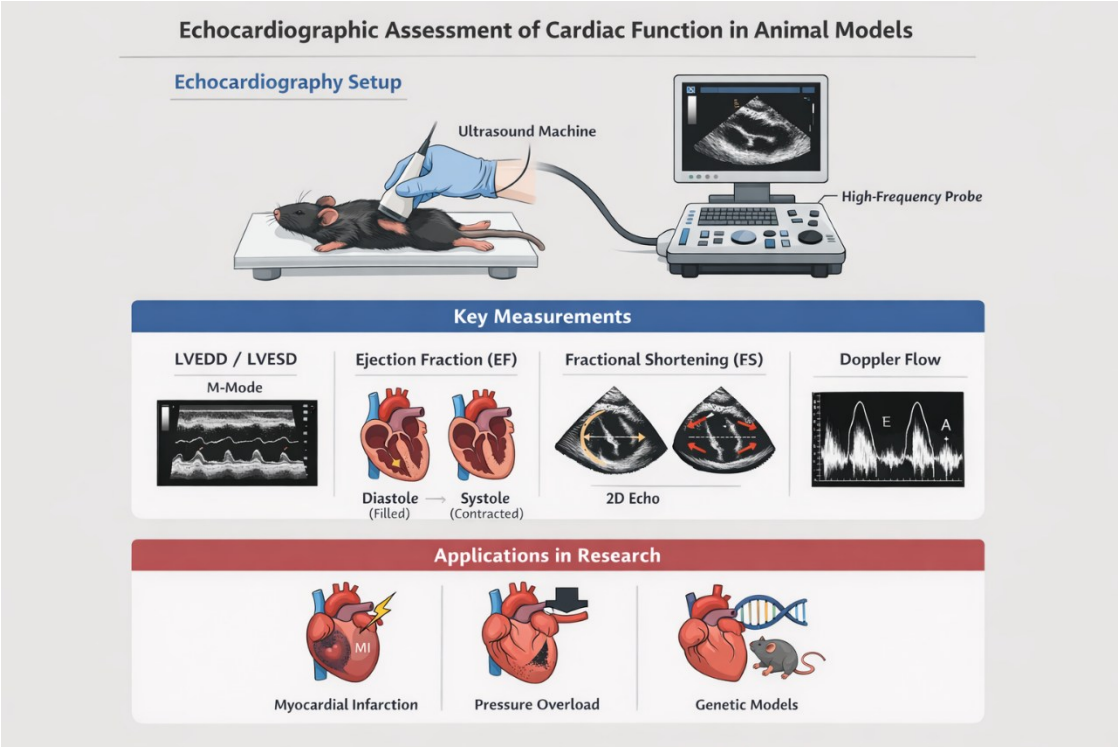

Figure 1.8. Echocardiographic assessment of cardiac function in animal models**.** Schematic representation of high-resolution ultrasound imaging used to evaluate cardiac structure and function in experimental animals. The figure illustrates probe positioning, visualization of cardiac chambers, and commonly assessed functional parameters, including ventricular dimensions, systolic performance, and blood flow patterns. Figure created by the author for illustrative purposes using AI (ChatGPT 2026, OpenAI).

Chapter 2 - Aim of the Work

Platelet-derived growth factor receptor alpha (PDGFRα) identifies a population of cardiac stromal cells that play a central role in myocardial remodeling following injury. These cells have been widely associated with fibrotic responses, as they can differentiate into myofibroblasts and contribute to extracellular matrix (ECM) deposition in response to pathological stimuli such as ischemia and inflammation. Transforming growth factor-β (TGFβ) signaling represents a key pathway driving this profibrotic activation.

However, recent evidence suggests that PDGFRα$^+$ cells are not exclusively pathological, but may also participate in tissue repair processes, including vascular remodeling and maintenance of myocardial integrity. This highlights a potential dual role of PDGFRα$^+$ cells in the injured heart, contributing both to maladaptive fibrosis and to beneficial regenerative responses. The mechanisms regulating this balance remain poorly understood.

The primary aim of this study was to investigate the functional role of PDGFRα$^+$ cells in cardiac remodeling following ischemia/reperfusion (I/R) injury, with particular focus on their contribution to the balance between fibrosis and revascularization. To address this, an inducible PDGFRα$^+$ cell ablation model was employed to evaluate the impact of these cells on cardiac function, extracellular matrix deposition, cardiomyocyte remodeling, and vascular density in vivo.

In addition, this study aimed to explore the molecular mechanisms underlying PDGFRα-associated fibrotic signaling. Specifically, we investigated the contribution of clathrin-mediated intracellular trafficking pathways in regulating profibrotic responses. These mechanisms were examined using pharmacological inhibition approaches in porcine cardiac PDGFRα$^+$ cells, focusing on key fibrosis-associated genes.

By integrating *in vivo* functional analyses with *ex vivo* molecular studies, this work aims to provide a comprehensive understanding of the dual role of PDGFRα$^+$ cells in cardiac injury and repair. Ultimately, these findings may contribute to the development of therapeutic strategies that selectively limit fibrosis while preserving or enhancing cardiac regenerative capacity.

Chapter 3 - Material and Methods

3.1 Mouse Strains and Breeding

To generate an inducible PDGFRα^{+} cell ablation model, PDGFRα–MerCreMer mice were crossed with diphtheria toxin A (DTA) reporter mice.

The PDGFRα–MerCreMer line expresses tamoxifen-inducible Cre recombinase under control of the PDGFRα promoter, enabling temporal regulation of recombination in PDGFRα-expressing cells. The DTA reporter line carries a loxP-flanked STOP cassette upstream of the diphtheria toxin A gene, allowing Cre-dependent expression of DTA and subsequent cell ablation.

Genotyping was carried out by PCR analysis of genomic DNA extracted from tail biopsies collected at postnatal day 30.

Experimental groups included:

- PDGFRα–MerCreMer/DTA+/+ (ablation group): This group was treated with tamoxifen and represents the experimental condition where PDGFRα cells are conditionally ablated.
- PDGFRα–MerCreMer; DTA+/− (control group): This group represents Cre and DTA mice separately and serves as the control and was also treated with tamoxifen.

Age and sex matched littermates were included in all experiments. All mice were derived from a C57BL/6 background, which guarantees genetic uniformity and compatibility across the strains. Breeding and experiments took place in a controlled environment free from specific pathogens, within the institutional animal facility. These activities were carried out in line with ethical animal welfare protocols that received approval from the institutional committee.

3.2 Ischemia–Reperfusion (I/R) Surgery

Three, four months old mice were anesthetized with 5% isoflurane in oxygen until loss of the righting reflex and subsequently maintained at 1.5–2% isoflurane delivered at 1.5, O_2 via a nose cone. Adequate depth of anesthesia was verified by the absence of withdrawal reflex in response to toe pinch. Throughout the procedure, body temperature was continuously maintained at 37°C using a thermostatically controlled heating pad.

A 0.5 cm median cervical incision was performed under sterile conditions, and the underlying tissues were carefully dissected to expose the trachea. The lobes of the thyroid gland were gently separated to facilitate visualization. The trachea was intubated using a sterile cannula (Harvard Apparatus), which was connected to a small-animal ventilator set to deliver 260 μL tidal volume at a rate of 130 breaths per minute.

A left thoracotomy was performed through an incision between the third and fourth intercostal spaces to expose the heart. Ischemia–reperfusion (I/R) injury was induced by temporary ligation of the left anterior descending (LAD) coronary artery using a 6-0 silk suture placed around a PE-10 tubing. Coronary occlusion was maintained for 20 minutes, after which the ligature was released to allow reperfusion. The chest cavity was closed in layers using 6-0 silk sutures. Mice were extubated upon recovery of spontaneous respiration and monitored until fully ambulatory.

For postoperative analgesia, Ethiqua XR (3.25 mg/kg) was administered subcutaneously prior to recovery and subsequently every 48 hours as required. Control mice did not undergo sham thoracotomy or coronary ligation. Baseline mice were not subjected to surgical procedures.

3.3 Tamoxifen-Induced Cell Ablation

To induce Cre-mediated recombination and selective ablation of PDGFRα^+ cells, tamoxifen (TAM) was administered beginning seven days after I/R injury. Mice receive tamoxifen once daily for five consecutive days. Control of animals received PBS. Animals were analyzed seven days after the final tamoxifen injection.

Mice were generated by knocking the tamoxifen inducible *Cre-ER* cDNA into the *Pdgfrα* locus. MCM mice were maintained in a hemizygous state and crossed with *DTA-flox* reporter mice. *DTA-flox* mice *(Jackson Laboratories; strain B6.129P2-Gt(ROSA)26Sor$^{tm1(DTA)Lky}$/J, JAX stock # 009669)* have Cre-inducible expression of the human DTA that renders cells susceptible to ablation following recombination. *MCM^{+}/DTA$^{+/+}$* mice were treated with 2mg tamoxifen (Sigma Aldrich, T5648) diluted in peanut oil (Sigma Aldrich). For control groups, *MCM+* mice lacking *DTA* and *DTA+/+* mice lacking Cre were treated with tamoxifen under identical conditions for five consecutive days. Immunofluorescence and histochemistry staining, confocal microscopy and collection of whole cardiac tissue for spatial transcriptomics were performed at different time points after I/R induction.

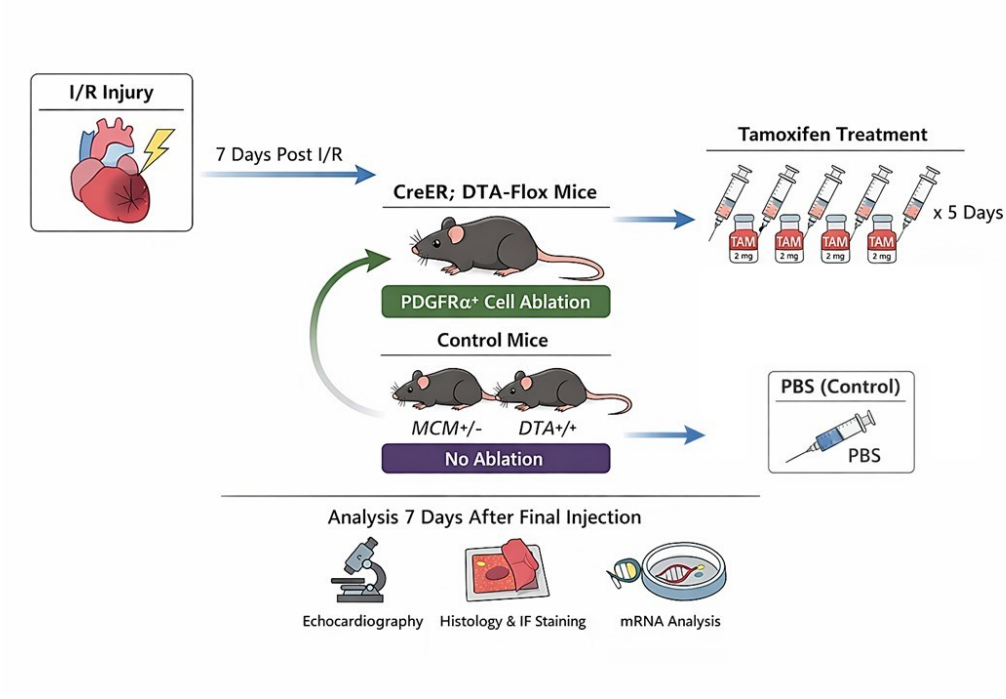

Figure 3.1. Diagram illustrating the steps for inducing I/R injury, ablation, and further analysis. Figure created by the author for illustrative purposes using AI (ChatGPT 2026, OpenAI).

3.4 Echocardiographic Assessment

Cardiac function was assessed by transthoracic echocardiography in anesthetized mice using a high-resolution micro-ultrasound imaging system (Vevo 2100, Visual Sonics, Toronto, Canada) equipped with a high-frequency linear array transducer (22–55 MHz) at the Biomedical Engineering and Imaging Institute at Icahn School of Medicine at Mount Sinai.

Figure 3.2. Vevo 2100 micro-ultrasound imaging system (VisualSonics, Toronto, Canada) used for transthoracic echocardiography. Image adapted from manufacturer's website

Mice were anesthetized with 1–2% isoflurane and positioned supine on a temperature-controlled platform maintained at 37 °C. Electrocardiogram electrodes were attached to monitor heart rate, which was maintained between 450–550 bpm to minimize anesthesia-induced cardiac depression. The thorax was shaved and pre-warmed ultrasound gel was applied to ensure optimal acoustic coupling. Two-dimensional (B-mode) images were acquired in parasternal long-axis and short-axis views. M-mode recordings were obtained at long axis to measure left ventricular (LV) internal diameters at end-diastole (LVEDD) and end-systole (LVESD), interventricular septal thickness, and posterior wall thickness. Left ventricular ejection fraction (LVEF), fractional shortening and left ventricular mass were calculated using VevoLab software from the average of two to three consecutive cardiac cycles. All analyses were performed by blinded operator to genotype and treatment group.

3.5 Tissue Collection and Processing

Cardiac tissue was harvested from control and ischemic mice, washed in PBS and fixed in 4% paraformaldehyde (PFA) to further process for paraffin sectioning or for embedding in OCT to prepare samples for frozen sections. Sections were collected from comparable anatomical regions (apex to base) for consistency. Paraffin-embedded cardiac tissues were sectioned at a thickness of 8 μm using a rotary microtome.

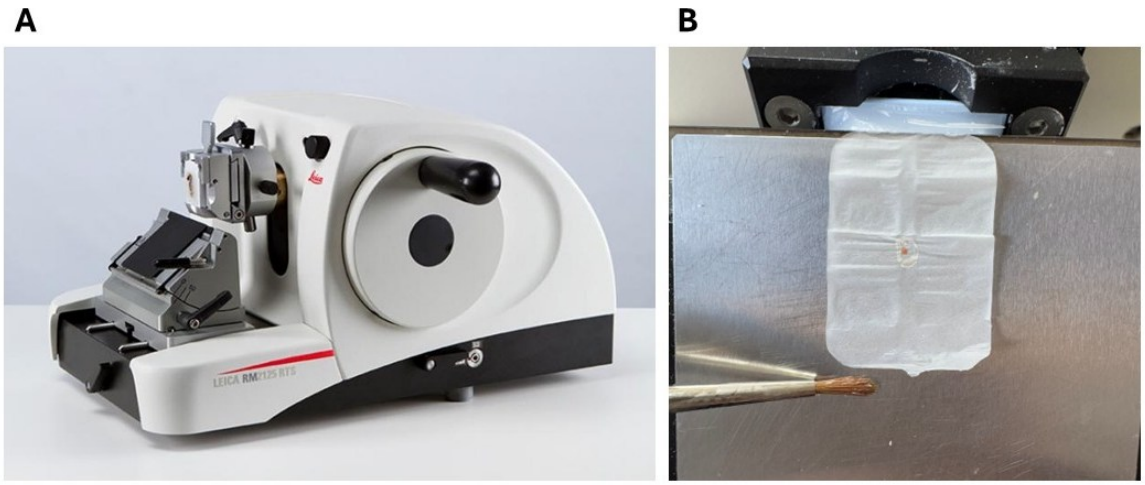

Figure 3.3. Paraffin sectioning using a rotary microtome. (A) Representative image of a rotary microtome (Leica) used for sectioning paraffin-embedded cardiac tissue. Image adapted from the manufacturer's website. (B) Preparation of paraffin tissue sections mounted on glass slides prior to staining. Image acquired by the author

3.6 Picrosirius Red Staining and Fibrosis Quantification

We stained both paraffin embedded and frozen sections heart, they sectioned at 8 μm thickness and processed for staining. Paraffin-embedded heart sections were deparaffinized, rehydrated, and stained with Picrosirius Red solution.

Sirius red was made with 0.5 grams of Picrosirius Red F3B stock and 500 ml of saturated aqueous solution of Picric acid, then we followed the protocol for treating paraffin embedded slide:

1) Dewax and hydrate paraffin sections
    a) put two times in Xylene, each time 10 minutes
    b) 100% ethanol, 5 minutes
    c) 80% ethanol, 5 minutes
    d) 70% ethanol, 5 minutes

2) Stain in Picrosirius Red for 1 hour.
3) Wash it two time in acidified water (5 ml Acetic acid in 1 liter of water), each for 5 minutes.
4) Dehydrate sections
    a) 70% ethanol, 5 minutes
    b) 80% ethanol, 5 minutes
    c) 100% ethanol, 10 minutes
    d) put two times in Xylene, each time 10 minutes

5) Mount sections by mounting solution and put cover slip

We also set up a protocol for assessing picrosirius red in frozen slides:

1. Let slides dry on bench top
2. Wash them with PBS
3. Put them in Xylene for 40 seconds
4. Put them in a mix of 50% ethanol 50% Xylene for 40 seconds
5. Put them in 100% ethanol for 40 seconds
6. Put them in 90% ethanol for 40 seconds
7. Put them in 70% ethanol for 40 seconds
8. Put them in 50% ethanol for 40 seconds
9. Fix them in 4% paraformaldehyde for 15 minutes
10. Do a quick wash with PBS, followed by a quick wash with deionized water
11. Put in 50% ethanol for 10 seconds
12. Put slides in diluted picrosirius red for 30 minutes
13. Put slides in picrosirius red for 40 minutes
14. Wash them with acetic acid 0.5% two times, each time 40 seconds
15. Wash them two times with 100% ethanol, each time 40 seconds
16. Put them in mix of 50% ethanol 50% Xylene for 40 seconds
17. Put in Xylene for 5 minutes.

Bright-field images were acquired using a light microscope and processed using LAS X software (Leica Microsystems). Fibrotic area was quantified using Fiji (ImageJ, NIH) by calculating the percentage of positively stained area relative to total tissue area.

3.7 Immunofluorescence staining

For immunofluorescence we used the following antibodies against: DAPI, CD31 (BD Bioscience, 550274), and WGA (Thermo Fisher, W11262). Secondary antibodies were purchased from Life Technologies and used at 1:100 or 1:200 dilution for 2 hours at room temperature.

Confocal microscopy was performed using a Leica SP8at the University of Pavia Core Facility and images were acquired as z-stacks on 10 µm frozen sections

For frozen sections, we followed this protocol:

1. Take samples from -80 and let them dry.
2. Wash with PBS three times, each time 5 minutes
3. Fix the samples in 4% paraformaldehyde (PFA) for 15 minutes.
4. Wash three times with PBS, each time for 5 minutes.
5. Triton 0.1%-PBS, 5 minutes.
6. Incubate sections in blocking buffer (2.5% donkey serum, 2.5% goat serum, 0.3% BSA, 0.1% Triton-PBS) for 60 minutes in humified chamber.
7. Dilute primary antibody in blocking buffer (4 um CD31, 2um WGA in 200 um blocking buffer), incubate it in humified chamber overnight at 4 degrees of centigrade.
8. Wash three times with 0.1& Triton-PBS, each time 5 minutes.
9. Dilute secondary antibody in 0.1% Triton-PBS and apply it to section for 2 hours (2 um in 200 um).
10. Wash them twice with 0.1% Triton-PBS, each time for 5 minutes.
11. Wash them with PBS, 5 minutes
12. Incubate with DAPI diluted in X1000 PBS for 7 minutes.

13. Mount it with mounting media and put cover slip on it and keep it in 4 degrees centigrade.

For paraffin sections we followed this protocol:

1. Wash with Xylene three times, each time 5 minutes
2. Wash with 100% ethanol, 10 minutes.
3. Wash with 80% ethanol, 10 minutes.
4. Wash with 70% ethanol, 10 minutes.
5. Wash with 50% ethanol, 10 minutes.
6. Wash with Deionized water two times, each time 5 minutes.
7. For antigen retrieval use a boiling water system in a glass coupling jar filled with antigen retrieval buffer (10mM sodium citrate buffer), where slides were immersed and boiled for 10 minutes
8. Let the slides cool down on bench top for 30 minutes.
9. Wash with distilled water for 5 minutes.
10. Wash with PBS, 5 minutes.
11. Treat withTriton 0.3%-PBS three times, each for 10 minutes.
12. Incubate sections in blocking buffer (2.5% donkey serum, 2.5% goat serum, 0.3% BSA, 0.3% Triton-PBS) for 30 minutes in humified chamber.
13. Dilute primary antibody in blocking buffer (4 ul CD31, 2ul WGA in 200 um blocking buffer), incubate it in humified chamber overnight at 4 degrees of centigrade.
14. Wash three times with 0.3% Triton-PBS, each time 5 minutes.
15. Dilute secondary antibody in 0.3% Triton-PBS and apply it to section for 2 hours (2 um in 200 um).
16. Wash them twice with 0.3% Triton-PBS, each time for 5 minutes.
17. Wash them with PBS, 5 minutes
18. Incubate with DAPI diluted in X1000 PBS for 10 minutes.
19. Wash them with PBS three times, each time for 5 minutes.
20. Mount it with mounting media and put cover slip on it and keep it in 4 degrees centigrade.

3.8 Confocal microscopy

MCM^{+}*/DTA*$^{++}$ cardiac tissue preparations were imaged at the Core Facility of the University of Pavia. Confocal images were acquired using a Leica SP8, whereas histochemistry analysis was performed using a Leica DMi8 WF/TIRF Microscope. Tile scans were acquired and computationally stitched to generate high-resolution composite images of entire cardiac sections.

3.8 Flow Cytometry

For flow cytometric analysis we used different antibodies depending on the experimental procedures. For flow cytometry cell sorting of porcine PDGFRα cells we used PE-conjugated anti-human PDGFRα (BioLegend, #323505). For analysis of the ablation samples, we used APC-conjugated PDGFRα (eBioscience, #17-1401-81).

For all flow cytometry analysis, hearts were harvested after PBS 1X perfusion to remove blood from the ventricular cavities and atria and aortic tissue removed. Samples were minced in 1ml of serum free DMEM containing 0.8 Wunsch units/ml of Liberase DH (Roche Diagnostic, #743337) and left for 30 minutes at 37°C on a shaking thermoblock at 1200rpm. Samples were further treated with 1x RBC lysis buffer (Thermo Fisher Scientific # 00-4333) as indicated by the manufacturer's instructions. Removal of debris was performed by serial passages into 70 μm and 40 μm filters. Cells were incubated for 1 hour with specific antibodies diluted at 1μg per million cells in PBS containing 2% BSA. Dead cells were excluded by labeling with 1μg/ml of DAPI 5 minutes prior analysis. Sorting of the porcine PDGFRa cells was performed at the Flow Cytometry Core Facility at Icahn School of Medicine, Mount Sinai.

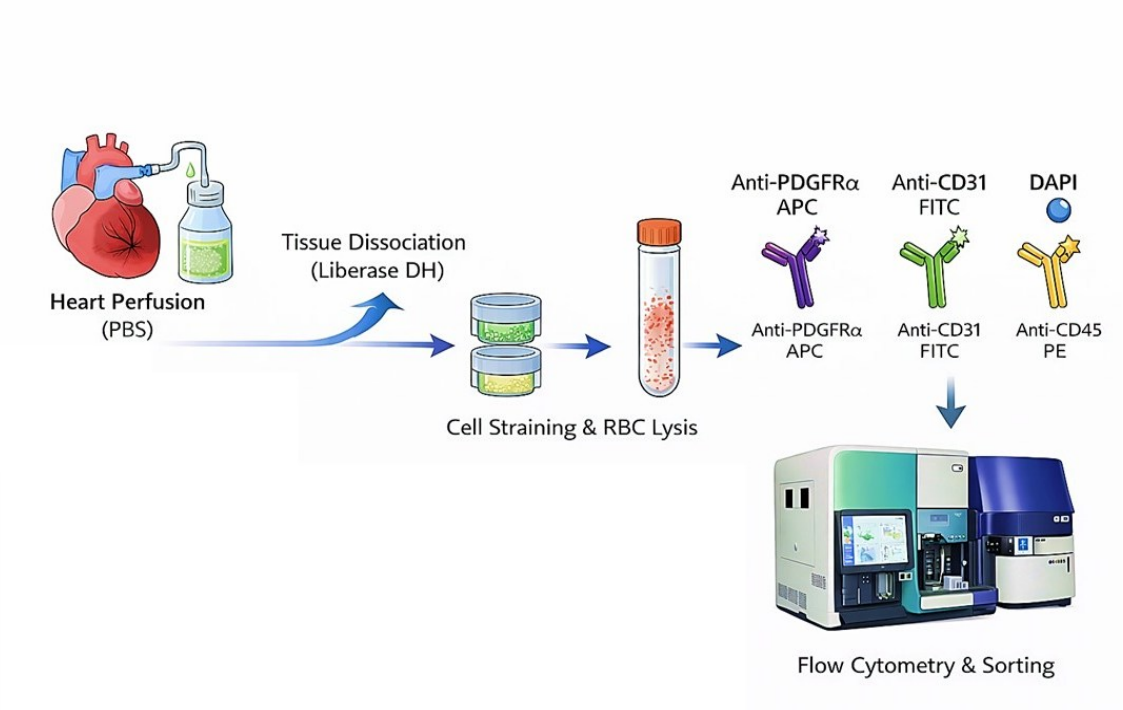

Figure 3.4. Workflow of cardiac tissue dissociation and flow cytometry analysis. Cardiac tissues were perfused with PBS by intra-ventricular injection, harvested, and enzymatically digested with Liberase DH (Roche) to generate single-cell suspensions. Cells were filtered, treated with RBC lysis buffer, and stained with fluorochrome-conjugated antibodies against PDGFRα, along with DAPI for viability assessment. Samples were analyzed and sorted using flow cytometry platforms. *Figure created by the author for illustrative purposes using AI (ChatGPT 2026, OpenAI).*

3.9 Porcine Tissue Collection

We used porcine PDGFRα^{+} cells from the heart of 4 control Yorkshire pigs 4-5 months old in use for different experiments. The animals were euthanized immediately after the echocardiographic and hemodynamic assessment. The heart was quickly removed, and the great vessels were dissected. The atria were carefully separated from the ventricular chambers. The right ventricular

free wall was dissected, and 1mm^3 biopsy were collected to extract PDGFRα$^+$ cells. Minced biopsies were digested with Liberase DH (Roche Diagnostic, 743337) at different concentrations.

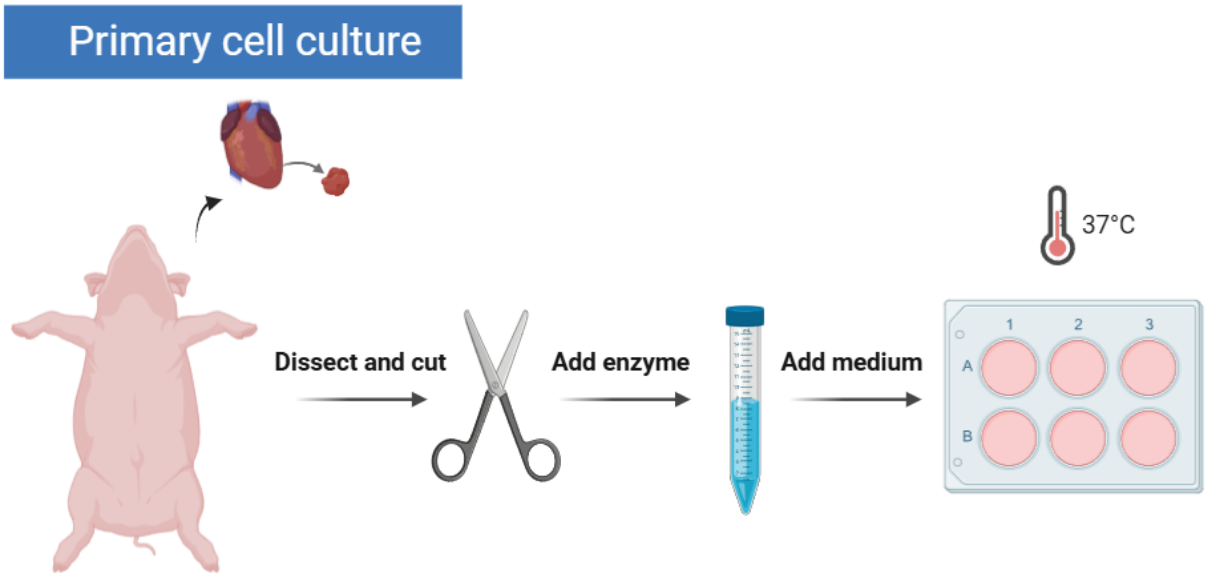

Figure 3.5. Schematic representation of primary cardiac cell isolation and culture. Cardiac tissue was harvested and dissected into small fragments, followed by enzymatic digestion to obtain a cell suspension. Cells were subsequently resuspended in culture medium and plated under standard conditions at 37°C for primary cell culture. *Figure created by the author for illustrative purposes with Biorender.*

3.10 Porcine Cardiac Cell Culture

Biopsies were minced and plated for 3 days to allow cells to attach to plastic in a 6 multiwell. After cell attachment, media was changed daily till cells reached confluency. Cells were trypsinazed and prepared for flow sorting. FACS-sorted PDGFRα$^+$ cells were expanded for further experiments. Cells were plated in hypoxic conditions (5% O_2) in DMEM (low glucose-Glutamax 10-567-014

Fisher Scientific) supplemented with 1% antibiotic/antimycotic (15-240-096 Fisher Scientific). and 10% FBS (A5670701 Fisher Scientific). Cells were used for experiments at passage 4-6 or when colony forming units were visible at every trypsin-mediated detachment.

Cell treatment occurred after 12 hours starvation in DMEM/LG-Glutamax supplemented in 0.5%serum. TGFβ (PeproTECH, #100-21-2UG) was used for the indicated time length at 10ng/ml, whereas Chlorpromazine (Millipore Sigma, #C8137) was used at 5μg/ml for 6 hours.

3.11 TGFβ and Chlorpromazine Treatment

We treated 3 or 4 cell clones from porcine cardiac left ventricle with chlorpromazine and/or TGFβ to assess whether chlorpromazine can block the clathrin-mediated pathway. We had three conditions for each cell culture, starvation, TGFβ, and TGFβ with chlorpromazine.

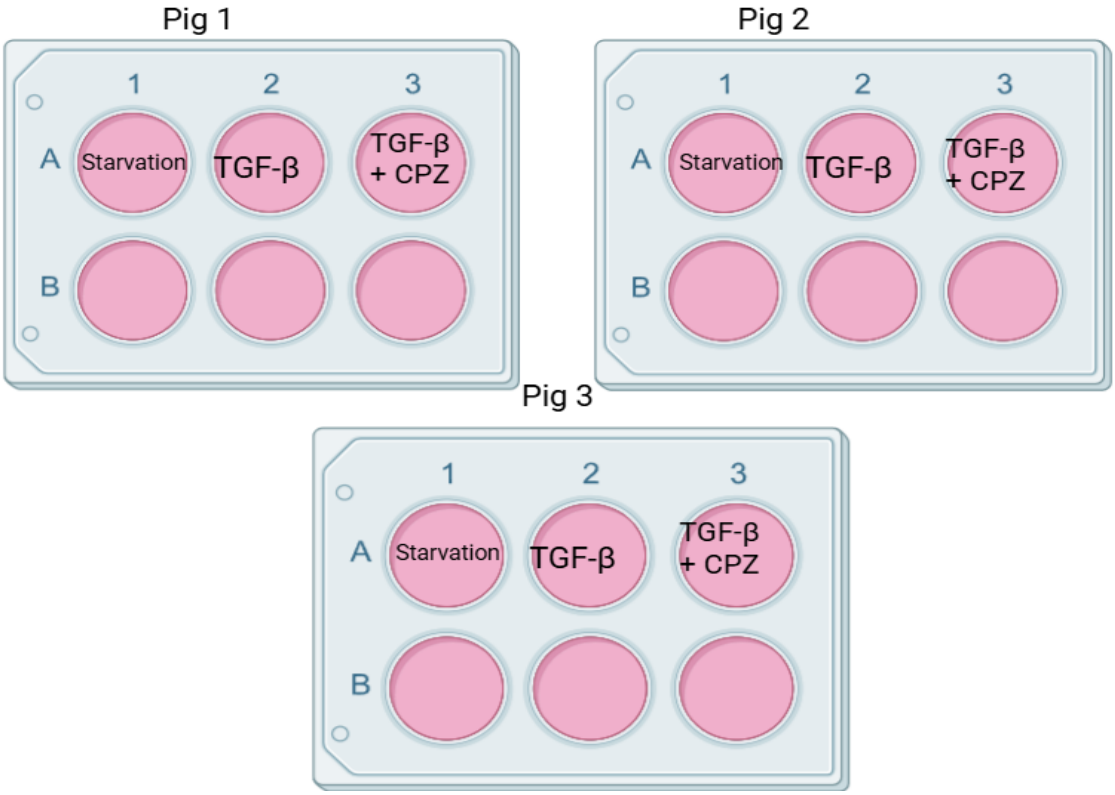

Figure 3.6. Experimental design of porcine cardiac cell treatments**.** Primary cardiac cells isolated from four or three independent porcine samples (Pig 1–4) were cultured and subjected to different treatment conditions. Cells were either serum-starved (0.5% serum), treated with TGFβ (10 ng/mL), and co-treated with TGFβ (10 ng/mL) and chlorpromazine (5 µg/mL). Each well represents a specific treatment condition within the multiwell plates.

3.12 RNA Isolation, cDNA analysis and RT-qPCR

RNA was extracted from porcine PDGFRα^{+} cells using a RNAeasy mini kit (Qiagen) as described by the manufacturer.

Figure 3.7 RNA extraction RNease Mini Kit from Quaigen.

RNA was measured using a Nanodrop 2000c (Thermo Scientific). The relative quantity of a particular transcript can be determined by qPCR using a highly expressed internal standard, such as 18S ribosomal subunit or GAPDH as a reference. The amount of the corresponding cDNA is directly proportional to the amount of the mRNA of interest in the original RNA sample.

The most robust and widely used technique to study mRNA transcript abundance in whole organs, tissues or specific cells is real-time polymerase chain reaction (qPCR). As the name indicates, this technique is based on specific sequence amplification by PCR. To achieve this, two separate reactions are required. First, the mRNA sequence needs to be reversely transcribed into complementary DNA (cDNA). This process is non-specific, meaning that a cDNA copy is generated for every polyadenylated strand of RNA present. cDNA is synthesized by the commercial enzyme Multiscribe® Reverse Transcriptase which is a recombinant protein derived from Moloney murine leukemia virus reverse transcriptase

cDNA was synthesized using a TaqMan reverse transcription kit (Applied Biosystems).

Figure 3.8. Multiscribe reverse transcriptase kit from Applied Biosystem (Thermofisher)

component	volume
RT buffer (10X)	1.0 µl
Random Hexamers (50 µM)	0.5 µl
dNTP Mixture (10 mM)	2.0 µl
MgCl2 Solution (25 mM)	2.2 µl
RNase inhibitor	0.2 µl
Multiscribe® MuLV Reverse Transcriptase	0.625 µl
Nuclease Free H2O	0.475 µl
RNA (100 ng/ µl)	1 µl
Total Volume	10 µl

Table 3.1. Recipe for cDNA synthesis. All reagents were supplied with the MultiScribe® reverse transcription kit (Applied biosystems, 43-665-96)

RNA samples stored at -80 °C were thawed on ice. The reverse transcription reaction was setup on ice using the chemicals shown in 3.1 briefly, a master mix was prepared containing all components except the RNA and was aliquoted into nuclease-free PCR tubes. RNA was added in the last step and the tubes loaded on a PHC-3 Thermal Cycler (Techne Bibbi Scientific, Stone, UK). Thermocycler conditions for cDNA synthesis are displayed in 3.2.

Stage	**Duration**	**Temperature (Centigrade)**
1 cycle	10 minutes	25
	30 minutes	48
	5 minutes	95

Table 3.2. Thermocycler program for cDNA synthesis.

Real-time polymerase chain reaction (qPCR) was performed using Fast optical tubes and 96-well plates (0.1 mL, Applied Biosystems, 4346907) and Taqman® Fast Advanced Master Mix (Applied Biosystems, 4444557). A master mix for all samples was prepared according to table 3.3 and aliquoted into the reaction wells.

Components	**Volume**
Taqman Fast Advanced Master Mix	10 µl
18S Reference (20X)	1 µl
GOI Probe (20X)	1 µl
Nuclease free H2O	5 µl
cDNA (2 ng/ µl)	3 µl
Total Volume	20 µl

Table 3.3. Recipe list for fast real-time PCR reactions.

Finally, cDNA samples were added, the plates sealed using optical adhesive film (Applied Biosystems, 4313663) and centrifuged for 3 minutes at 1500 g to remove any air bubbles from the bottom of each well potentially introduced during pipetting. Table 3.4 shows the cycler conditions for the qPCR reaction.

Stage	*Temperature*	*Time*
Hold	95	10 minutes
	95	15 seconds
40 cycles	60	60 seconds

Table 3.4. Thermo cycle program for Fast qPCR reactions.

The probe for the gene of interest (GOI) is frequently labelled with the reporter dye FAM™ at the 5‟ end and a non-fluorescent quencher (NFQ) as well as minor grove binder (MGB) situated at the 3‟ end. FAM™ is fluorescent dye emitting light at 520 nm upon excitation. In the native state of the probe, NFQ suppresses FAM™ fluorescence by Förster-type energy transfer (Förster 1948). MGBs increase melting temperature (Tm) and hence allow for design of shorter probes.

category	gene	purpose	Assay ID
House keeping	S18	Normalization	Cat NO. 4333760T
Fibrosis marker	SERPINE1	ECM remodeling	Ss03392656_u1
Fibrosis marker	Col1A1	Myofibroblast activation marker	Ss03373340_m1
Myofibroblast marker	CNN1	Marker of contractile phenotype	Ss03392449_g1
Fibrosis marker	ACTA2	ECM remodeling	Ss04245588_m1

Table 3.5. A summary table of primer sequences, gene targets, and functional categories is included.

A reference probe, labelled with a 5‟ VIC® reporter dye and a TAMRA™ quencher at the 3‟ end, is used for simultaneous analysis with the target gene a process referred to as duplex rtPCR. Upon excitation, VIC emits light at 580 nm. Following hybridisation of each probe to their respective

target cDNA, DNA polymerase cleaves off the FAM™ or VIC™ labels during the PCR reaction. Without quenching, free FAM™/VIC® emit a detectable fluorescent signal. The intensity of light emitted can be directly correlated to the number of target strands in the reaction. The cycle at which the emitted light reaches a certain threshold (set at the beginning of the linear range) defines the cycle threshold (C_T). The C_T of the GOI is normalised against the C_T of a housekeeping gene, the expression of which must not be affected by the experiment (i.e. the drug used to treat the cells or animals). The housekeeping gene used throughout this study was the 18s ribosomal subunit.

Chapter 4 - Results

4.1 Experimental design and timeline for inducible cell ablation following ischemia–reperfusion injury

To observe the role of PDGFRα^{+} cells in cardiac remodeling we performed cell ablation following I/R injury using an inducible genetic mouse model. This system uses mice expressing Cre-ERT2 under PDGFRα promoter [*PdgfrαMerCreMer (MCM)]* crossed with transgenic mice expressing the diphtheria toxin subunit A (DTA) allele *(B6.129P2-Gt (ROSA)26Sor$^{tm1(DTA)Lky}$/J)* to generate MCM^{+}/DTA^{++} mice. We induced I/R injury to analyze the myocardial issue response and function in absence of PDGFRα^{+} cells. Seven days after I/R, tamoxifen administration was initiated to activate MerCreMer-mediated recombination (activate Cre into the nucleus and recombine floxed site). Tamoxifen was injected once daily for five consecutive days to induce Cre-dependent expression of diphtheria toxin A (DTA) and subsequent cell ablation (Figure 4.1).

Seven days after the final tamoxifen injection, cardiac function was assessed by transthoracic echocardiography, followed by tissue collection for histological and molecular analyses. This experimental timeline allowed separation of the acute injury phase from the genetic ablation phase, enabling evaluation of the effects of inducible cell ablation during sub-acute cardiac remodeling rather than during the immediate ischemic response. Indeed, we observed that ablation prior I/R induction caused 10% survival of the ablated mice with 90% of mice not surviving the 4th day after ischemia due to cardiac wall rupture and profuse bleeding in the thoracic cavity.

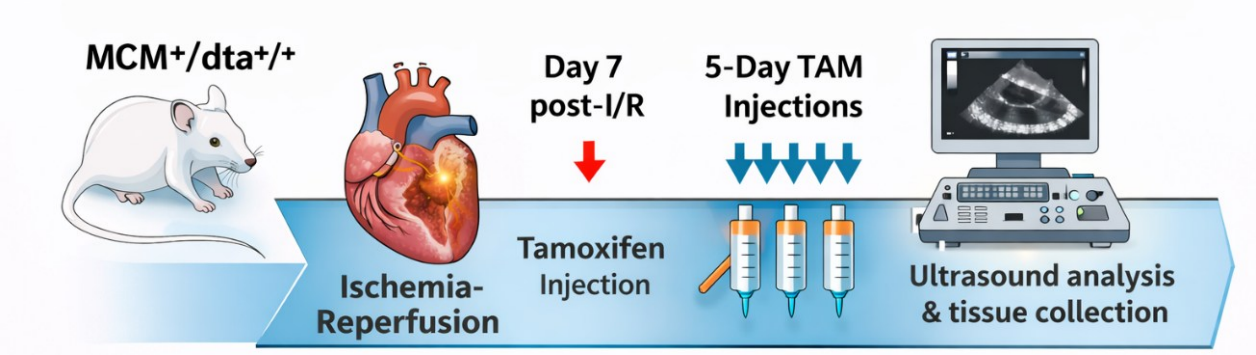

Figure 4.1. Experimental timeline for inducible cell ablation following ischemia–reperfusion injury**.** Schematic representation of the experimental design in MCM^{+}/DTA^{++} mice. Animals were subjected to ischemia–reperfusion (I/R) injury, followed by tamoxifen (TAM) administration starting 7 days post-I/R for five consecutive days to induce Cre-mediated recombination and cell ablation. Cardiac function was assessed by ultrasound analysis, and tissues were collected 7 days after the final tamoxifen injection. *Figure created by the author for illustrative purposes using AI (ChatGPT 2026, OpenAI).*

4.2 Validation of PDGFRα^{+} cell ablation following tamoxifen administration

To validate the efficiency of tamoxifen-induced genetic ablation, flow cytometry was performed to quantify PDGFRα^{+} cells in cardiac tissue. A sequential gating strategy was applied to exclude debris (Figure 4.2A) and non-viable cells (identified as DAPI^{+} cells; Figure 4.2B), followed by identification of PDGFRα-expressing populations after labelling with PDGFRα-APC conjugated antibody (Figure 4.2C).

Controls were included in the group of mice with genotype PDGFRα–MerCreMer or DTA$^{+/+}$ mice, whereas the ablation group included MCM^{+}/DTA^{++} genotype. Controls and ablation mice were

both treated with tamoxifen to exclude from the analysis the effect of this drug. In control mice a distinct population of PDGFRα^{+} cells were readily detected (Figure 4.2C). In contrast, tamoxifen-treated ablation mice exhibited a marked reduction (50-60%) in the PDGFRα^{+} cell population (Figure 4.2C-D). These data confirm effective tamoxifen-induced ablation of PDGFRα^{+} cells *in vivo*.

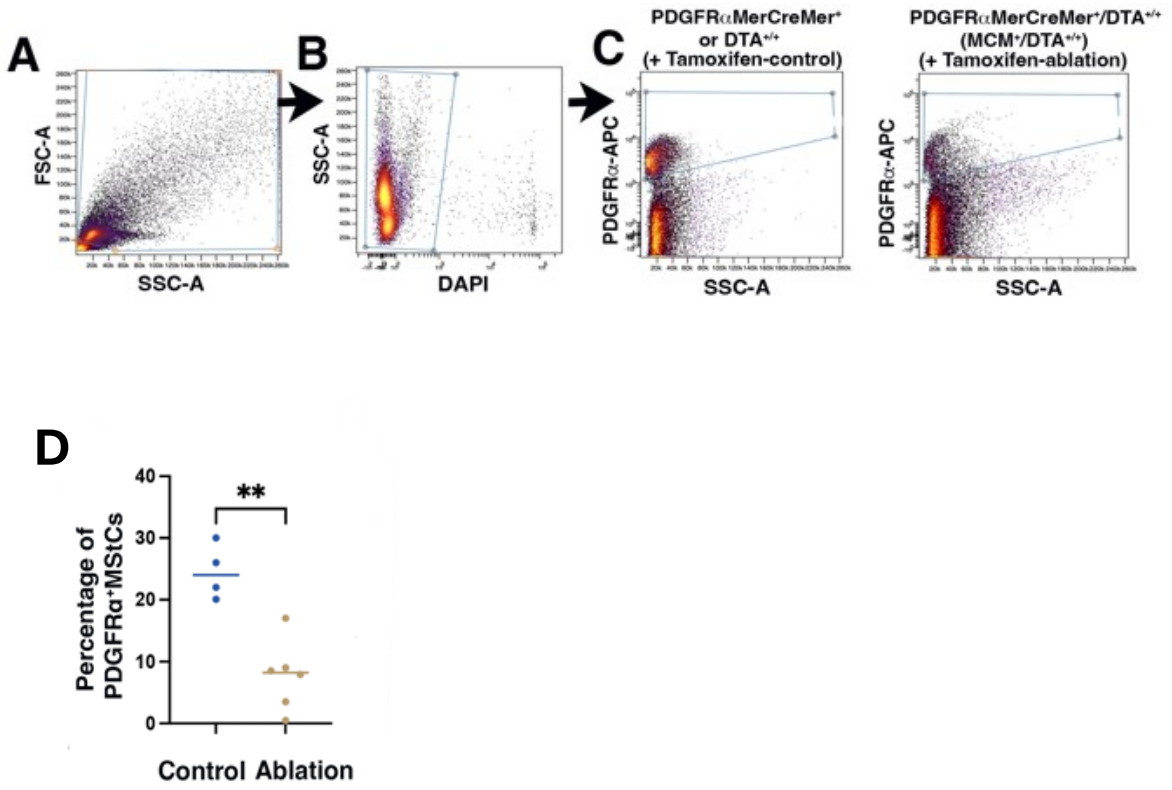

Figure 4.2 Tamoxifen-induced ablation efficiently depletes PDGFRα^{+} cells in the heart. Flow cytometry analysis of cardiac cells following tamoxifen treatment. (A) Forward scatter (FSC-A) versus side scatter (SSC-A) plot showing exclusion of debris. (B) DAPI staining used to exclude non-viable cells. (C) Identification of PDGFRα^{+} cells in tamoxifen-treated control mice (PDGFRα–MerCreMer; DTA$^{+/+}$).
and ablated mice (MCM^{+}/DTA$^{+/+}$) **(D)** Quantification of PDGFRa cells present in the heart in tamoxifen-treated control and ablated mice. The latter showed a marked reduction in PDGFRα^{+} cells. ** indicates significant changes with p,0.01, n=4 mice for controls and 6 mice for ablation.

4.3 Inducible cell ablation exacerbates systolic dysfunction following ischemia–reperfusion injury

Cardiac function was assessed by transthoracic echocardiography seven days after completion of tamoxifen treatment. Ejection fraction and fractional shortening were used as indices of left ventricular systolic performance. Under baseline conditions, ablation mice exhibited preserved systolic and diastolic function compared to control mice (Figure 4.3A-B). Importantly, I/R injury led to a marked decrease in systolic function in control mice. Notably, mice subjected to both I/R injury and inducible ablation exhibited severe systolic dysfunction comparable to that observed in control I/R mice (Figure 4.3A–B), indicating that PDGFRα^{+} cell ablation did not improve cardiac function following ischemic injury.

In contrast, left ventricular mass, as recorded by echocardiography and normalized to body weight, decreased moderately but significantly in ablation *versus* control group after I/R (Figure 4.3C), indicating that the observed ischemic dysfunction in ablation mice was not accompanied by the overt hypertrophic remodeling normally present because of the progression of the infarction.

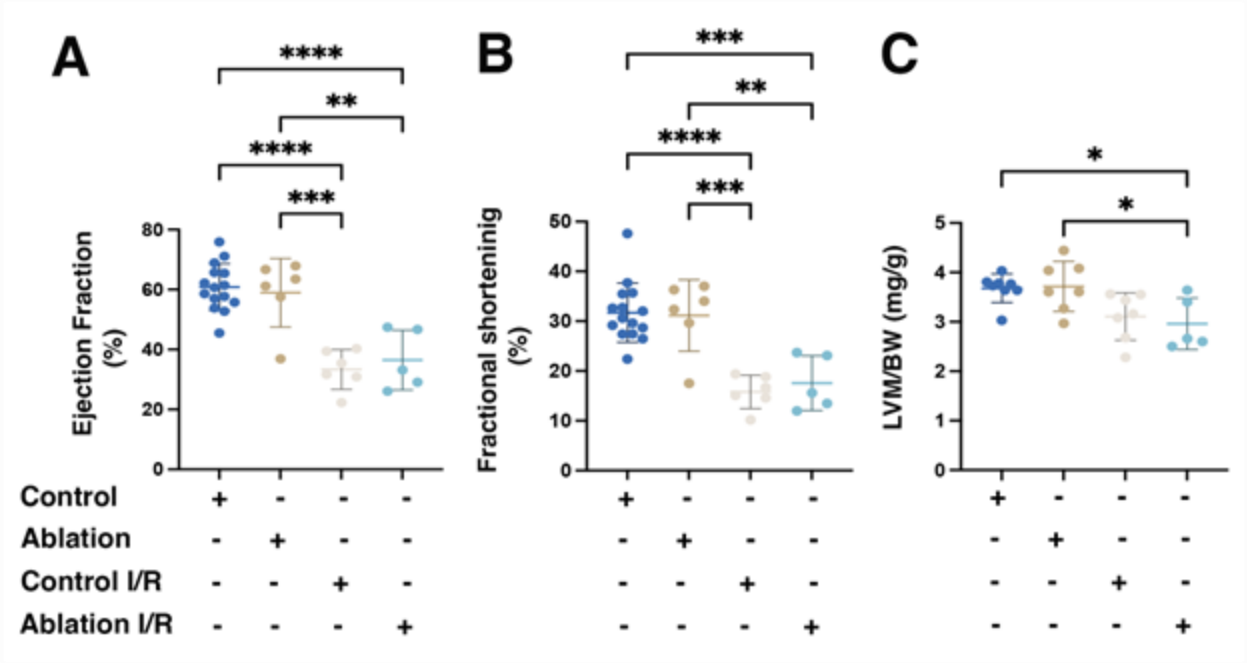

Figure 4.3. Inducible cell ablation exacerbates systolic dysfunction following ischemia–reperfusion. . Echocardiographic assessment of left ventricular systolic function in control and ablated mice under basal conditions and following I/R injury. (A) Left ventricular ejection fraction (EF, %) measured seven days after completion of tamoxifen treatment. (B) Fractional shortening (FS, %) measured at the same time point. (C) Left ventricular mass normalized to body weight (LVM/BW). Each data point represents an individual animal; bars indicate mean ± SD. Statistical significance was determined by One-way Anova followed by Tuckey comparison study. * indicates $p < 0.05$, ** $p < 0.01$, ***$p < 0.001$,**** $p < 0.0001$. n nuber is 15 for control baselin, 6 for ablation baseline, 7 for control I/R and 5 for ablation I/R.

4.4 Inducible cell ablation reduces fibrotic remodeling after I/R

To understand the functional data and their association to fibrotic and revascularization outcomes, we analyzed first the scar size throughout the whole heart in control and ablation mice after I/R. Cardiac fibrosis was assessed by Picrosirius Red which biochemically binds collagen fibers released by the myofibroblasts after ischemia. The data showed that control mice exhibited a

marked increase in fibrotic area compared with non-injured controls (Figure 4.4A-B). In contrast, inducible ablation resulted in a moderate but significant reduction in collagen deposition in the post-injury myocardium, suggesting that PDGFRα^{+} cell ablation may be beneficial in the subacute fibrotic response after I/R (Figure 4.4B).

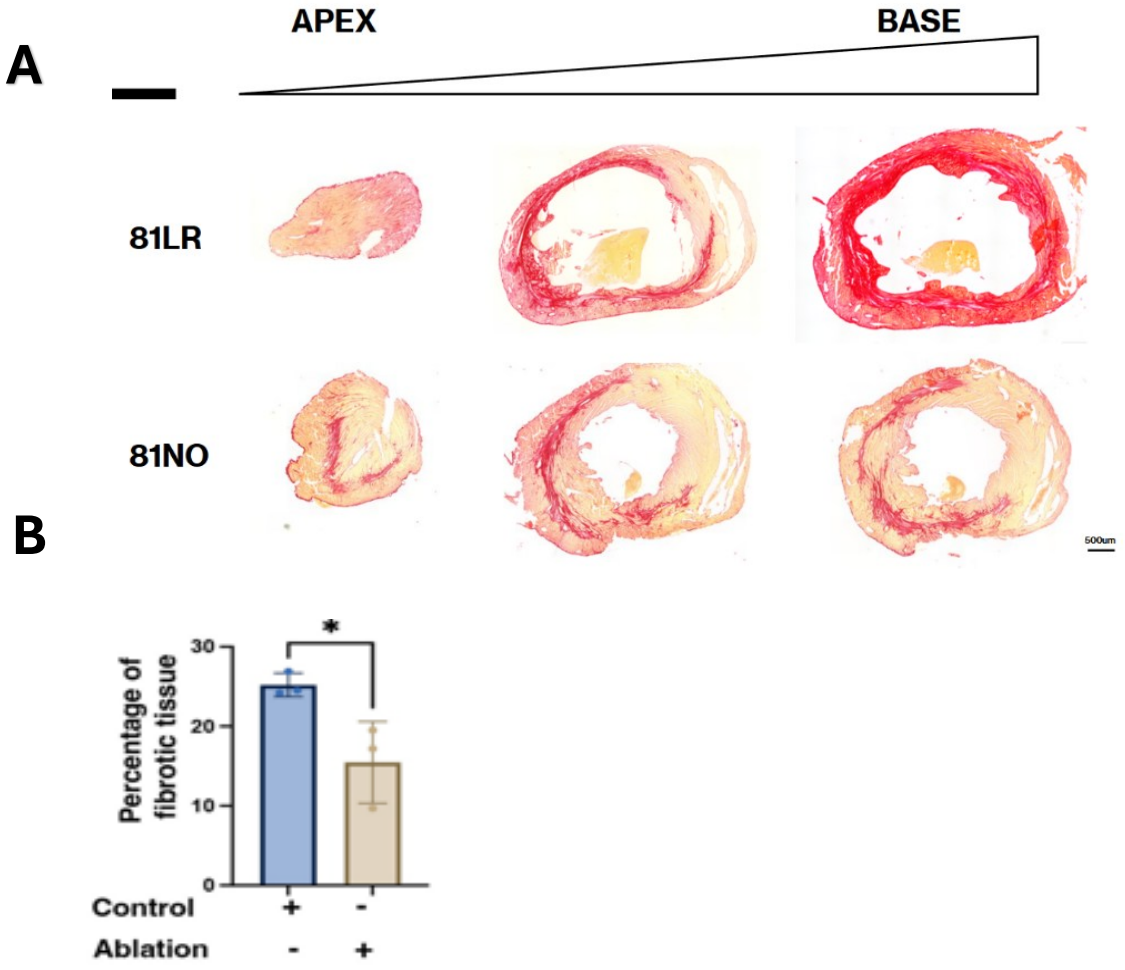

Figure 4.4. Inducible cell ablation reduces cardiac fibrosis following ischemia–reperfusion injury. (A) Representative Picrosirius Red staining of transverse heart sections from control I/R (81LR) and ablated I/R (81NO) mice, shown from apex to base. Collagen deposition is visualized in red. (B) Quantification of fibrotic area expressed as percentage of total myocardial area. We used 3

mice for each condition. Statistical analysis was performed by Student t-test. $p<0.05$. Scale bar: 500 μm.

4.5 Effects of inducible cell ablation on cardiomyocyte morphology and vascular density under physiological and pathological conditions

To understand the causal relationship between lack of cardiac function recovery, exacerbated ventricular mass accompanied by amelioration of the fibrotic response after ablation of PDGFRα^+ cells, we evaluated the impact of inducible cell ablation on cardiomyocyte morphology and vascular organization under both physiological and pathological conditions, measuring cardiomyocyte cross-sectional area (CSA) and capillary density.

Under physiological conditions, inducible ablation resulted in a modest increase in cardiomyocyte CSA compared with control hearts (Figure 4.5A-C). Following I/R injury, cardiomyocyte CSA significantly decreased in ablated hearts displaying a distinct reduction in the peri infarcted area (Figure 4.5A and D-E).

Analysis of vascular density revealed a significant lowering in the number of capillaries per cardiomyocyte in ablated hearts compared with controls under basal conditions (Figure 4.5F-H). This was exacerbated after I/R injury (Figure 4.5F and, I-J).

These findings demonstrate that inducible cell ablation affects both cardiomyocyte structural remodeling and vascular density under physiological conditions and exacerbates vascular rarefaction and cardiomyocytes response to ischemic conditions, explaining in part lack of cardiac function recovery and decreased ventricular mass.

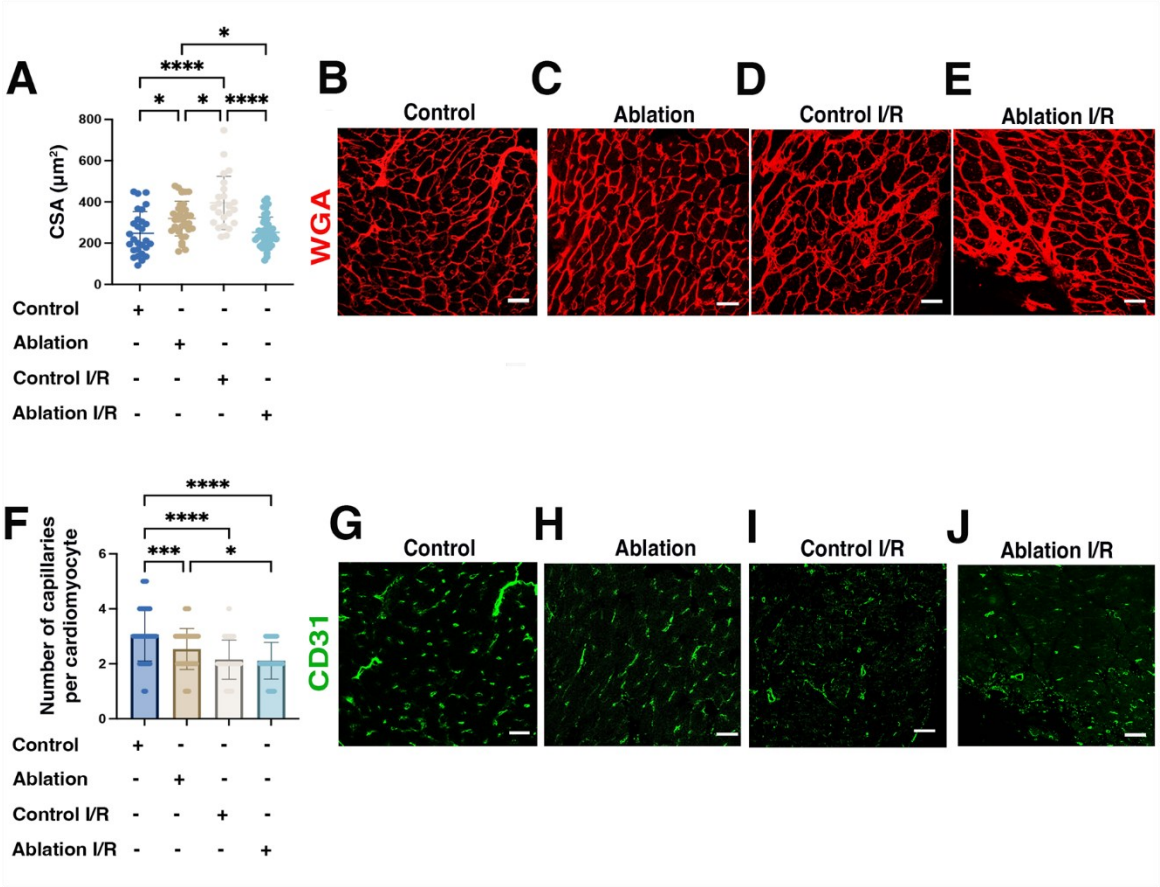

Figure 4.5. inducible cell ablation alters cardiomyocyte morphology and vascular density under physiological conditions. (A–B) Representative immunofluorescence images of left ventricular sections from control and ablated mice stained for wheat germ agglutinin (WGA; red), CD31 (G-J, green), and DAPI (blue). **(C)** Quantification of cardiomyocyte cross-sectional area (CSA). **(D)** Quantification of capillary density expressed as the number of capillaries per cardiomyocyte. Analysis was performed on 3 different animals and 10 fields in each section for 5 sections were used to measure capillary density and cross-sectional area. Statistical analysis was performed by One-way Anova followed by Tuckey comparisons.

4.6 Chlorpromazine modulates TGFβ-induced profibrotic gene expression in porcine PDGFRα + cells

Data presented in this thesis, conversely to previous analyses showed that ablation of PDGFRα$^+$ cells alleviated fibrosis, but deteriorated cardiomyocytes' response to ischemic conditions and exacerbated the revascularization program occurring after ischemia reperfusion. In contrast to Kuwabara and co-authors, our data does not associate ablation of PDGFRα$^+$ cells with possible therapeutic venues, claiming that control of fibrotic response mediated by these cells cannot be divided by their beneficial effects in tissue revascularization and cardiomyocytes integrity (ref Kuwabara). Using spatial transcriptomics analyses performed in Dr. Santini's laboratory at Icahn School of Medicine at Mount Sinai, in New York (data not shown), we analyzed Gene Ontology (GO) enrichment pathways (Reactome Pathways Annotation) to detect differentially expressed signaling identified in PDGFRα$^+$ cells at 3 and 7 days post-I/R, compared with physiological conditions. We observed that during the early acute phase after ischemia (3 days post-I/R) the fibrotic response in PDGFRα$^+$ cells was associated with clathrin-dependent signaling, which shifted into a transcriptomic profile involving contractile and elastic fiber assembly 7 days after I/R. To study this signaling, we collected 4 different biopsies from the porcine heart and generate by enzymatic digestion four different clones of PDGFRα$^+$ cells (Figure 4.6A). To investigate whether inhibition of clathrin-mediated endocytosis modulates TGFβ-driven profibrotic transcriptional responses, each of these clones was treated with TGFβ in the presence or absence of chlorpromazine, followed by RT–qPCR analysis of fibrosis-associated genes. A standardized workflow was established for tissue processing and downstream analyses, including left ventricular biopsy collection of four different pigs (Figure 4.6A), enzymatic dissociation of left ventricular biopsies, and cell attachment to the dish. Biopsies treated with high concentration of enzyme from Roche DHL had higher number of cells in the dish (Figure 4.6B). We further sort the cells expressing PDGFRα from the rest of the attached stromal cells by flow cytometry analysis (Figure 4.6D), using as control for gating strategy cells not labeled with PDGFRα PE-conjugated antibody (Figure 4.6C). After sorting, the cells were plated on a plastic 6 multi-well and as shown in Figure 4.6E, they formed colonies, which are indicative of mesenchymal cell features. Importantly, these cells did not express alfa-smooth muscle actin suggesting that they were not differentiated in myofibroblasts due to culture conditions and enzymatic treatment (Figure 4.6F).

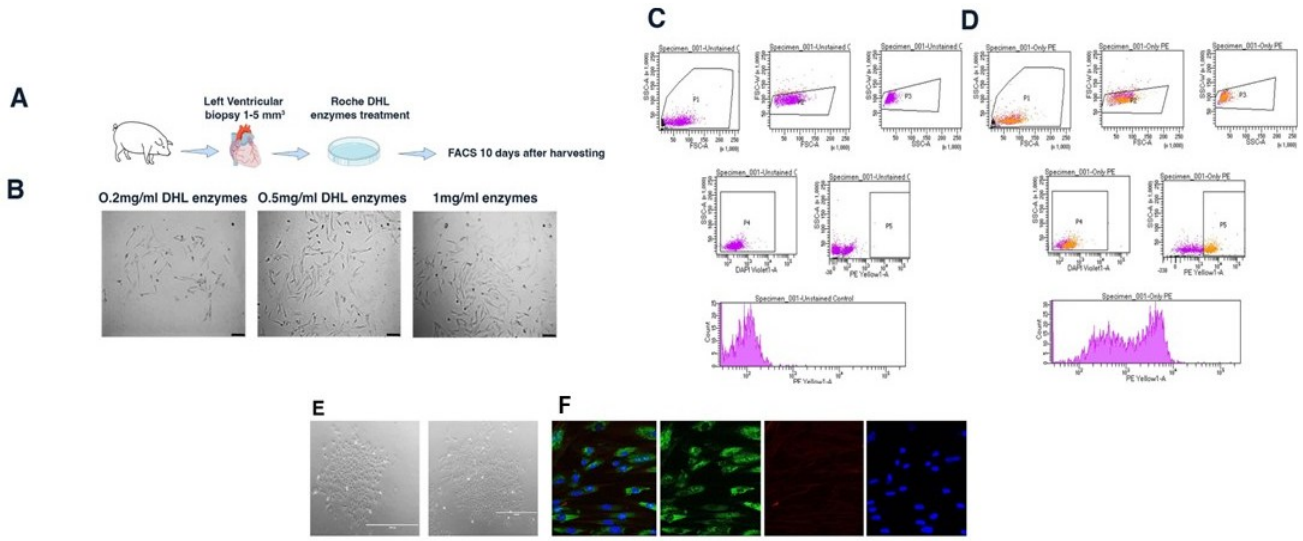

Figure 4.6. Workflow and quality control for porcine left ventricular tissue dissociation and downstream analyses. (A) Schematic overview of the experimental workflow. Left ventricular (LV) biopsies (1–5 mm³) were collected and enzymatically dissociated using Roche DHL enzyme mix, followed by downstream flow cytometry analysis performed 10 days after tissue harvesting. (B) Representative brightfield images illustrating the effect of different DHL enzyme concentrations (0.2, 0.5, and 1 mg/mL) on cell yield and morphology following LV tissue dissociation. (C) Flow cytometry gating strategy for unstained control samples, including sequential gates to exclude debris and define the main cell population based on forward and side scatter parameters. (D) Corresponding gating and signal distribution for single-stained PE control samples, illustrating fluorescence detection and thresholding relative to unstained controls. (E-F) Representative brightfield (E) and immunofluorescence (F) images of sorted cells, showing cellular morphology and colony formation. (F) PDGFRa expression (green) is localized in the cytoplasm, alfa-smooth muscle actin expression is lacking in early passages cells. DAPI was used to counterstain for nuclei (DAPI, blue). Scale bars are 100micrometersin B and E and 25 micrometers in F.

4.7 Chlorpromazine attenuates TGFβ-induced profibrotic gene expression in porcine cardiac tissue

To determine whether inhibition of clathrin-mediated endocytosis modulates TGFβ-driven profibrotic transcriptional responses, porcine cardiac cell clones were treated with TGFβ in the presence or absence of chlorpromazine, followed by RT–qPCR analysis. TGFβ stimulation resulted in increased expression of fibrosis-associated genes, including SERPINE1, and CNN1. Noteworthy ACTA2, which is the name of the gene alfa-smooth muscle actin, was also upregulated as early transcripts, further suggesting differentiation into a myofibroblast lineage (Figure 4.7). There was no significant increase in COL1A1 which means it could be counted as late genes in fibrosis response which could answer fibrosis later.

Co-treatment with chlorpromazine significantly attenuated TGFβ-induced upregulation of SERPINE1, and COL1A1 while expression of ACTA2 was not perturbated significantly (Figure 4.7). These data suggest a requirement for clathrin-dependent processes in mediating transcriptional responses leading to fibrosis but not differentiation into myofibroblasts and their contractile cytoskeletal system.

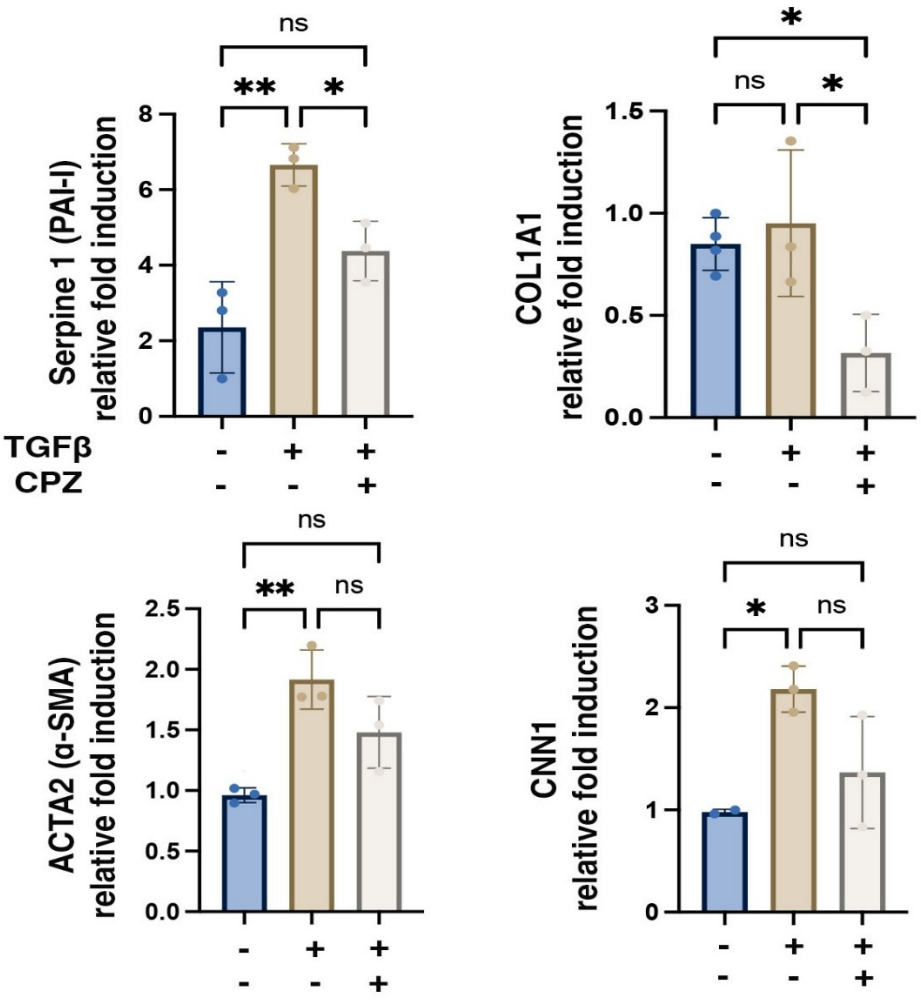

Figure 4.7. Chlorpromazine modulates TGFβ-induced profibrotic gene expression in porcine cardiac tissue. RT–qPCR analysis of fibrosis-associated genes in porcine cardiac cell clones in control conditions and following TGFβ stimulation with or without chlorpromazine treatment. Relative mRNA expression levels of CNN1, COL1A1, ACTA2, and SERPINE1 are shown. Gene expression was normalized to the housekeeping controls and expressed relative to S18 conditions. Data are presented as mean ± SD. Statistical significance is analyzed by One-way Anova followed by Tuckey comparison. * Indicates $p < 0.05$, ** $p < 0.01$, ns, not significant.

Chapter 5 - Discussion

Cardiac remodeling following ischemia–reperfusion (I/R) injury is a highly coordinated process involving the interplay between fibrotic deposition, vascular remodeling, and cardiomyocyte adaptation. While fibrosis has traditionally been viewed as a detrimental outcome of cardiac injury, increasing evidence suggests that fibrotic and regenerative processes are tightly interconnected and may be regulated by shared cellular populations (58). In this study, we investigated the role of PDGFRα$^+$ cells in this context and identified their context-dependent function in both physiological and pathological cardiac remodeling.

5.1 PDGFRα$^+$ cells contribute to cardiac homeostasis under basal conditions

Our data demonstrate that partial ablation of PDGFRα$^+$ cells under physiological conditions results in measurable structural alterations, including reduced capillary density and changes in cardiomyocyte cross-sectional area, despite the absence of overt systolic dysfunction. These findings indicate that PDGFRα$^+$ cells are not merely activated in response to injury but actively contribute to the maintenance of myocardial architecture and microvascular organization at baseline.

This observation supports the concept that PDGFRα$^+$ MStCs function as key regulators of the myocardial microenvironment. Their role likely extends beyond extracellular matrix production to include paracrine signaling mechanisms that sustain endothelial cell function and cardiomyocyte integrity (59). Therefore, even partial depletion of this cell population disrupts the equilibrium of the cardiac niche, leading to subtle but significant structural changes.

5.2 Ablation of PDGFRα⁺ cells reduce fibrosis but impairs cardiac repair after I/R

Following ischemia–reperfusion injury, PDGFRα⁺ cell ablation resulted in a modest but consistent reduction in fibrotic tissue deposition. This finding agrees with the well-established role of PDGFRα signaling in fibroblast activation and myofibroblast differentiation (60). PDGFRα⁺ cells represent a major source of collagen-producing cells, and their removal effectively limits extracellular matrix accumulation.

However, this antifibrotic effect did not translate into improved cardiac function. Instead, PDGFRα⁺ cell ablation was associated with reduced capillary density and decreased left ventricular mass, indicating impaired structural and vascular recovery. These findings highlight a critical paradox: while reducing fibrosis is generally considered beneficial, indiscriminate depletion of PDGFRα⁺ cells disrupt essential reparative processes.

This observation strongly supports the hypothesis that PDGFRα⁺ cells exert dual functions in cardiac remodeling. On one hand, they contribute to pathological fibrosis; on the other, they are required for effective tissue repair, including revascularization and maintenance of myocardial structure. Therefore, global targeting of this population may produce unintended consequences by eliminating both harmful and beneficial cellular (61).

5.3 PDGFRα⁺ cells as regulators of the balance between fibrosis and revascularization

One of the most significant findings of this study is the identification of PDGFRα⁺ cells as key mediators of the balance between fibrotic remodeling and vascular regeneration. The reduction in revascularization observed following PDGFRα⁺ cell ablation suggests that these cells contribute to the formation or stabilization of the cardiac microvasculature.

Previous studies have indicated that subsets of PDGFRα⁺ mesenchymal cells may possess pro-angiogenic properties or support endothelial cell survival through paracrine signaling (62). Our findings are consistent with this concept and further suggest that PDGFRα⁺ cells are required to orchestrate coordinated repair responses following injury. Their removal disrupts this balance,

leading to a state in which reduced fibrosis is accompanied by insufficient vascular support and compromised tissue integrity.

5.4 Clathrin-dependent trafficking as a regulator of fibrotic signaling

To further investigate the molecular mechanisms underlying PDGFRα-associated fibrotic responses, we performed complementary in vitro experiments using porcine cardiac stromal cells. Spatial transcriptomi gene ontology of cardiac murine hearts after ischemia-reperfusion (data not shown) suggested enrichment of clathrin-dependent trafficking pathways during early post-injury remodeling, implicating intracellular vesicular transport as a potential regulator of fibrotic signaling.

Clathrin-mediated endocytosis is known to regulate receptor internalization and downstream signaling, including pathways activated by growth factors such as TGFβ (63). In this context, receptor trafficking can influence signal duration, localization, and transcriptional output.

Consistent with this, pharmacological inhibition of clathrin-mediated endocytosis using chlorpromazine selectively attenuated TGFβ-induced SERPINE1 expression, while ACTA2 expression remained largely unaffected. This finding is particularly noteworthy, as TGFβ is a well-established inducer of both genes, yet their regulation appears to diverge at the level of intracellular signaling.

5.5 Spatial compartmentalization of TGFβ signaling

These results suggest that TGFβ signaling in PDGFRα^{+} cells is not a uniform process but rather involves spatially distinct signaling pathways. We propose that clathrin-dependent endosomal trafficking is required for the full activation of specific transcriptional programs, such as SERPINE1 expression, whereas other targets, including ACTA2, may be regulated through alternative signaling routes.

This model introduces the concept of intracellular trafficking as a regulatory checkpoint that modulates the specificity of fibrotic gene expression. Rather than acting as a global amplifier of TGFβ signaling, the endocytic machinery selectively controls distinct transcriptional outputs, thereby contributing to the fine-tuning of fibrotic responses.

5.6 Functional implications of selective SERPINE1 regulation

The selective modulation of SERPINE1 is particularly relevant in the context of cardiac fibrosis. SERPINE1 encodes plasminogen activator inhibitor-1 (PAI-1), a key regulator of fibrinolysis and extracellular matrix turnover. Elevated SERPINE1 levels contribute to matrix accumulation and fibrotic progression.

Therefore, the ability to selectively reduce SERPINE1 expression without affecting ACTA2-mediated myofibroblast differentiation suggests a potential therapeutic strategy. Targeting specific intracellular pathways may allow the attenuation of pathological matrix accumulation while preserving the structural functions required for scar stabilization.

5.7 Limitations of the study

Despite these findings, several limitations should be considered. First, the ablation model used in this study does not discriminate between distinct subpopulations of PDGFRα^{+} cells, which may exert different and potentially opposing functions. Second, while the *in vitro* experiments provide mechanistic insights, *in vivo* cardiac remodeling in presence of inhibitors of clathrin-dependent endosomal trafficking should be performed to validate the transcriptomic and *in vitro* data. Third, a human comparative analysis is still lacking. This should be frames for future pharmacological therapies.

Conclusion

In this study, we investigated the role of PDGFRα$^+$ cells in cardiac remodeling following ischemia–reperfusion injury and demonstrated their dual and context-dependent function. Ablation of PDGFRα$^+$ cells resulted in a reduction of fibrotic remodeling, confirming their contribution to extracellular matrix deposition. However, this effect was accompanied by decreased vascular density and alterations in cardiomyocyte structure, indicating impaired reparative processes and highlighting the essential role of these cells in maintaining cardiac integrity.

Mechanistically, our findings suggest that fibrotic signaling downstream of TGFβ is selectively regulated by intracellular trafficking pathways. Inhibition of clathrin-mediated endocytosis modulated SERPINE1 expression without affecting ACTA2, supporting the existence of distinct regulatory mechanisms controlling fibrotic gene programs.

Overall, these results indicate that PDGFRα$^+$ cells are not solely drivers of pathological fibrosis but are also critical contributors to cardiac repair. Therefore, therapeutic strategies targeting PDGFRα signaling should aim for selective modulation rather than complete inhibition, in order to reduce fibrosis while preserving essential regenerative functions.

References

1. Meijler F, Meijler T. Archetype, adaptation and the mammalian heart. Netherlands Heart Journal. 2011;19(3):142–8.
2. Jain V, Bordes SJ, Bhardwaj A. Physiology, pulmonary circulatory system. 2018.
3. Rehman I, Kerndt CC, Rehman A. Anatomy, thorax, heart left anterior descending (LAD) artery. StatPearls [Internet]: StatPearls Publishing; 2023.
4. Gordan R, Gwathmey JK, Xie L-H. Autonomic and endocrine control of cardiovascular function. World journal of cardiology. 2015;7(4):204.
5. Sundjaja JH, Bordoni B. Anatomy, thorax, heart pulmonic valve. 2019.
6. Ho S, Nihoyannopoulos P. Anatomy, echocardiography, and normal right ventricular dimensions. Heart. 2006;92(suppl 1):i2–i13.
7. Litviňuková M, Talavera-López C, Maatz H, Reichart D, Worth CL, Lindberg EL, et al. Cells of the adult human heart. Nature. 2020;588(7838):466–72.
8. Dewing JM, Saunders V, O'kelly I, Wilson DI. Defining cardiac cell populations and relative cellular composition of the early fetal human heart. PLoS One. 2022;17(11):e0259477.
9. Bowers SL, Meng Q, Molkentin JD. Fibroblasts orchestrate cellular crosstalk in the heart through the ECM. Nature cardiovascular research. 2022;1(4):312–21.
10. Lim GB. Complexity and plasticity of cardiac cellular composition. Nature Reviews Cardiology. 2020;17(12):759–.
11. Baena-Montes JM, Kraśny MJ, O'Halloran M, Dunne E, Quinlan LR. In Vitro Models for Improved Therapeutic Interventions in Atrial Fibrillation. Journal of Personalized Medicine. 2023;13(8):1237.
12. Hill JA, Olson EN. Cardiac plasticity. New England Journal of Medicine. 2008;358(13):1370–80.
13. Yeates K, Lohfeld L, Sleeth J, Morales F, Rajkotia Y, Ogedegbe O. A global perspective on cardiovascular disease in vulnerable populations. Canadian Journal of Cardiology. 2015;31(9):1081–93.
14. Di Cesare M, Perel P, Taylor S, Kabudula C, Bixby H, Gaziano TA, et al. The heart of the world. Global heart. 2024;19(1):11.

15. Mendis S, Graham I, Narula J. Addressing the global burden of cardiovascular diseases; need for scalable and sustainable frameworks. Global Heart. 2022;17(1):48.

16. Lopez EO, Ballard BD, Jan A. Cardiovascular disease. StatPearls [Internet]: StatPearls Publishing; 2023.

17. Hosseini K, Mortazavi SH, Sadeghian S, Ayati A, Nalini M, Aminorroaya A, et al. Prevalence and trends of coronary artery disease risk factors and their effect on age of diagnosis in patients with established coronary artery disease: Tehran Heart Center (2005–2015). BMC cardiovascular disorders. 2021;21(1):477.

18. Shahjehan RD, Sharma S, Bhutta BS. Coronary artery disease. StatPearls [Internet]: StatPearls Publishing; 2024.

19. Libby P. The changing landscape of atherosclerosis. Nature. 2021;592(7855):524–33.

20. Klabunde R. Cardiovascular physiology concepts: Lippincott Williams & Wilkins; 2011.

21. Frangogiannis NG. Cardiac fibrosis: Cell biological mechanisms, molecular pathways and therapeutic opportunities. Molecular aspects of medicine. 2019;65:70–99.

22. Tallquist MD, Molkentin JD. Redefining the identity of cardiac fibroblasts. Nature Reviews Cardiology. 2017;14(8):484–91.

23. Kong P, Christia P, Frangogiannis NG. The pathogenesis of cardiac fibrosis. Cellular and molecular life sciences. 2014;71(4):549–74.

24. Bertaud A, Joshkon A, Heim X, Bachelier R, Bardin N, Leroyer AS, et al. Signaling pathways and potential therapeutic strategies in cardiac fibrosis. International journal of molecular sciences. 2023;24(2):1756.

25. Kovacic JC, Dimmeler S, Harvey RP, Finkel T, Aikawa E, Krenning G, et al. Endothelial to mesenchymal transition in cardiovascular disease: JACC state-of-the-art review. Journal of the American College of Cardiology. 2019;73(2):190–209.

26. Frangogiannis NG. Transforming growth factor–β in tissue fibrosis. Journal of Experimental Medicine. 2020;217(3):e20190103.

27. Khalil H, Kanisicak O, Prasad V, Correll RN, Fu X, Schips T, et al. Fibroblast-specific TGF-β–Smad2/3 signaling underlies cardiac fibrosis. The Journal of clinical investigation. 2017;127(10):3770–83.

28. Bujak M, Frangogiannis NG. The role of TGF-β signaling in myocardial infarction and cardiac remodeling. Cardiovascular research. 2007;74(2):184–95.

29. Meng X-m, Nikolic-Paterson DJ, Lan HY. TGF-β: the master regulator of fibrosis. Nature Reviews Nephrology. 2016;12(6):325–38.
30. Rabieian R, Boshtam M, Zareei M, Kouhpayeh S, Masoudifar A, Mirzaei H. Plasminogen activator inhibitor type-1 as a regulator of fibrosis. Journal of cellular biochemistry. 2018;119(1):17–27.
31. Zhao K, Zhang J, Xu T, Yang C, Weng L, Wu T, et al. Low-intensity pulsed ultrasound ameliorates angiotensin II-induced cardiac fibrosis by alleviating inflammation via a caveolin-1-dependent pathway. Journal of Zhejiang University-Science B. 2021;22(10):818–38.
32. Hinz B. The role of myofibroblasts in wound healing. Current research in translational medicine. 2016;64(4):171–7.
33. Liu R, Jin J-P. Calponin isoforms CNN1, CNN2 and CNN3: Regulators for actin cytoskeleton functions in smooth muscle and non-muscle cells. Gene. 2016;585(1):143–53.
34. Silvestre J-S, Smadja DM, Levy BI. Postischemic revascularization: from cellular and molecular mechanisms to clinical applications. Physiological reviews. 2013;93(4):1743–802.
35. Chung N, Lydakis C, Belgore F, Blann A, Lip G. Angiogenesis in myocardial infarction. An acute or chronic process? European heart journal. 2002;23(20):1604–8.
36. Demoulin J-B, Essaghir A. PDGF receptor signaling networks in normal and cancer cells. Cytokine & growth factor reviews. 2014;25(3):273–83.
37. Heldin C-H, Lennartsson J. Structural and functional properties of platelet-derived growth factor and stem cell factor receptors. Cold Spring Harbor perspectives in biology. 2013;5(8):a009100.
38. Papadopoulos N, Lennartsson J, Heldin C-H. PDGFRβ translocates to the nucleus and regulates chromatin remodeling via TATA element–modifying factor 1. Journal of Cell Biology. 2018;217(5):1701–17.
39. Li D, Huang L-T, Zhang C-p, Li Q, Wang J-H. Insights into the role of platelet-derived growth factors: implications for Parkinson's disease pathogenesis and treatment. Frontiers in Aging Neuroscience. 2022;14:890509.
40. Andrae J, Gallini R, Betsholtz C. Role of platelet-derived growth factors in physiology and medicine. Genes & development. 2008;22(10):1276–312.

41. Farahani RM, Xaymardan M. Platelet-derived growth factor receptor alpha as a marker of mesenchymal stem cells in development and stem cell biology. Stem cells international. 2015;2015(1):362753.
42. Donovan J, Abraham D, Norman J. Platelet-derived growth factor signaling in mesenchymal cells. Front Biosci (Landmark Ed). 2013;18(1):106–19.
43. Michelis KC, Nomura-Kitabayashi A, Lecce L, Franzén O, Koplev S, Xu Y, et al. CD90 identifies adventitial mesenchymal progenitor cells in adult human medium-and large-sized arteries. Stem cell reports. 2018;11(1):242–57.
44. Santini MP, Malide D, Hoffman G, Pandey G, D'Escamard V, Nomura-Kitabayashi A, et al. Tissue-resident PDGFRα+ progenitor cells contribute to fibrosis versus healing in a context- and spatiotemporally dependent manner. Cell Reports. 2020;30(2):555–70. e7.
45. Chong JJ, Chandrakanthan V, Xaymardan M, Asli NS, Li J, Ahmed I, et al. Adult cardiac-resident MSC-like stem cells with a proepicardial origin. Cell stem cell. 2011;9(6):527–40.
46. Chong JJ, Reinecke H, Iwata M, Torok-Storb B, Stempien-Otero A, Murry CE. Progenitor cells identified by PDGFR-alpha expression in the developing and diseased human heart. Stem cells and development. 2013;22(13):1932–43.
47. Deshmukh T, Hume RD, Chen S, Igoor S, Foster SL, Barry T, et al. Platelet derived growth factor-AB modulates post-infarct myocardium leading to extended improvement in cardiac function. npj Regenerative Medicine. 2025;10(1):46.
48. Thavapalachandran S, Grieve SM, Hume RD, Le TYL, Raguram K, Hudson JE, et al. Platelet-derived growth factor-AB improves scar mechanics and vascularity after myocardial infarction. Science translational medicine. 2020;12(524):eaay2140.
49. Hsieh PC, Davis ME, Gannon J, MacGillivray C, Lee RT. Controlled delivery of PDGF-BB for myocardial protection using injectable self-assembling peptide nanofibers. J Clin Invest. 2006;116(1):237–48.
50. Noseda M, Harada M, McSweeney S, Leja T, Belian E, Stuckey DJ, et al. PDGFRalpha demarcates the cardiogenic clonogenic Sca1+ stem/progenitor cell in adult murine myocardium. Nat Commun. 2015;6:6930.
51. Lindsey ML, Bolli R, Canty Jr JM, Du X-J, Frangogiannis NG, Frantz S, et al. Guidelines for experimental models of myocardial ischemia and infarction. American Journal of Physiology-Heart and Circulatory Physiology. 2018;314(4):H812–H38.

52. Kim H, Kim M, Im S-K, Fang S. Mouse Cre-LoxP system: general principles to determine tissue-specific roles of target genes. Laboratory animal research. 2018;34(4):147–59.

53. Nagy A. Cre recombinase: the universal reagent for genome tailoring. genesis. 2000;26(2):99–109.

54. Foster MP, Benedek MJ, Billings TD, Montgomery JS. Dynamics in Cre-loxP site-specific recombination. Current opinion in structural biology. 2024;88:102878.

55. Sohal DS, Nghiem M, Crackower MA, Witt SA, Kimball TR, Tymitz KM, et al. Temporally regulated and tissue-specific gene manipulations in the adult and embryonic heart using a tamoxifen-inducible Cre protein. Circulation research. 2001;89(1):20–5.

56. Hoit BD, Castro C, Bultron G, Knight S, Matlib MA. Noninvasive evaluation of cardiac dysfunction by echocardiography in streptozotocin-induced diabetic rats. Journal of cardiac failure. 1999;5(4):324–33.

57. Lang RM, Badano LP, Mor-Avi V, Afilalo J, Armstrong A, Ernande L, et al. Recommendations for cardiac chamber quantification by echocardiography in adults: an update from the American Society of Echocardiography and the European Association of Cardiovascular Imaging. European Heart Journal-Cardiovascular Imaging. 2015;16(3):233–71.

58. Talman V, Ruskoaho H. Cardiac fibrosis in myocardial infarction—from repair and remodeling to regeneration. Cell and tissue research. 2016;365(3):563–81.

59. Ivey MJ, Tallquist MD. Defining the cardiac fibroblast. Circulation Journal. 2016;80(11):2269–76.

60. Ivey MJ, Kuwabara JT, Riggsbee KL, Tallquist MD. Platelet-derived growth factor receptor-α is essential for cardiac fibroblast survival. American Journal of Physiology-Heart and Circulatory Physiology. 2019;317(2):H330–H44.

61. Kaesler N, Babler A, Floege J, Kramann R. Cardiac remodeling in chronic kidney disease. Toxins. 2020;12(3):161.

62. Liu H, Ma Y, Chen N, Guo S, Liu H, Guo X, et al. Overexpression of stress-inducible OsBURP16, the β subunit of polygalacturonase 1, decreases pectin content and cell adhesion and increases abiotic stress sensitivity in rice. Plant, Cell & Environment. 2014;37(5):1144–58.

63. Chen C-L, Hou W-H, Liu I-H, Hsiao G, Huang SS, Huang JS. Inhibitors of clathrin-dependent endocytosis enhance TGFβ signaling and responses. Journal of cell science. 2009;122(11):1863–71.

Acknowledgements

I would like to express my sincere gratitude to all the people who contributed to this work and supported me throughout my Master's thesis.

First and foremost, I would like to thank my supervisor, Professor. Maria Paola Santini, for giving me the opportunity to be part of her research group. I am deeply grateful for her scientific guidance, continuous support, patience, and encouragement throughout this project. Her knowledge, critical thinking, and dedication to research have greatly influenced my scientific growth.

My sincere thanks also go to Raima Ramesh, Rana Najafi and all the members of the laboratory for their collaboration and for providing part of the experimental data and scientific expertise that contributed to this project.

I am deeply grateful to my family for their unconditional love, encouragement, and endless support throughout my academic journey. Their belief in me has always been my greatest source of motivation, especially during the most challenging moments.

Finally, I would like to thank all my friends and colleagues who supported me, encouraged me, and shared this journey with me. Their friendship and understanding made this experience even more meaningful.

This thesis represents not only the completion of my Master's degree but also an important step in my scientific and personal development. I am sincerely grateful to everyone who has contributed to this achievement.